https://doi.org/10.1016/j.ces.2019.115373
This is the Pre-Published Version.

Optimization and control of energy saving side-stream extractive distillation with heat integration for separating ethyl acetate-ethanol azeotrope

Tao Shi[1,2], Wei Chun[3], Ao Yang[1,2], Yang Su[1,2], Saimeng Jin[1,2], Jingzheng Ren[4] and Weifeng Shen[1,2,*]

[1]School of Chemistry and Chemical Engineering, Chongqing University, Chongqing 400044, P. R. China

[2]National-municipal Joint Engineering laboratory for Chemical Process Intensification and Reaction, Chongqing University, Chongqing 400044, P. R. China

[3]School of Economics and Business Administration, Chongqing University, Chongqing 400044, P. R. China

[4]Department of Industrial and Systems Engineering, The Hong Kong Polytechnic University, Hong Kong SAR, P. R. China

Corresponding Author: *(W.S) E-mail: shenweifeng@cqu.edu.cn

Abstract:

Currently, limited efforts have focused on the multi-objective optimization and effective control of the side-stream extractive distillation processes (EDS). Herein, the EDS and a heat-integration scheme (EDSH) are proposed for separating the minimum-boiling azeotropic mixture ethyl acetate (EtAC)-ethanol (EtOH). Firstly, the conceptual design by residue curve maps is demonstrated for the EDS. Following which, the genetic algorithm (GA) optimization is carried out to minimize the total capital investment cost (CAP) and the annual energy cost (ENR). Optimal scheme under the product purity constraints is then obtained from the Pareto front. And the EDSH scheme is shown with less TAC and CO2 emission. Therefore, an improved control structure CS3 combining the composition-(RR1/SIDE) cascade and feedforward strategy is developed to achieve decent dynamic responses for the EDSH. The anti-disturbance capability of different control structures in terms of the transient deviation and offsets are compared with the assistance of the integral absolute error.

Keywords: Side-stream extractive distillation; Conceptual design; Optimization; Dynamic

© 2019. This manuscript version is made available under the CC-BY-NC-ND 4.0 license http://creativecommons.org/licenses/by-nc-nd/4.0/

control

1. Introduction

Among the chemical industrial processes, it is impossible to obtain high-purity products by using conventional distillation for the separation of azeotropes. Therefore, advanced distillation processes such as pressure swing distillation (Liang *et al.,* 2017; Luyben, 2013a; Zhu *et al.,* 2016), azeotropic distillation (Chien *et al.,* 2004; Han *et al.,* 2019; Hegely and Lang, 2018) and extractive distillation (ED) (An *et al.,* 2015; Shen *et al.,* 2013; Shen *et al.,* 2015; Shen and Gerbaud, 2013) have been widely explored. It has been demonstrated that ED is one of the most promising methods for separating such azeotropic mixtures in the chemical industry and a comprehensive and systematic review of the ED process was studied by Gerbaud et al. (2019). With the aim of achieving lower energy consumption, intensified ED processes were extensively investigated. For instance, Yang *et al.* (2018) creatively presented an energy-saving strategy for the extractive dividing wall column (EDWC) in separating the multi-azeotropes heterogeneous mixtures with less equipment investment and lower energy cost. Yi *et al.* (2018) further investigated an energy-efficient process combining an extractive column and a regular distillation column. By integrating the vapor recompression heat pump and EDWC technologies in the bioethanol dehydration, Luo *et al.* (2015) achieved the purpose of saving more energy by 40% than the conventional scheme. Tututi-Avila *et al.* (2017) reported an energy-efficient ED system with side-stream (EDS) for separating binary azeotropes. And this alternative scheme can be further explored to allow the heat integration and achieve the gratifying dynamic performance.

More specifically, the new EDS process is an attractive structure to overcome the remixing effect and repeated separation path (Cui *et al.,* 2019). Additionally, there are further energy-saving improvements for separating the ethyl acetate (EtAC) and ethanol (EtOH) mixture when the side-stream ED process is considered. And the application of the heat-integration technology in the distillation process enables enormous economic benefits as well as lower energy consumption (Gu *et al.,* 2018; Luyben, 2008). Generally, the heat-integration in the pressure-swing distillation can be achieved when the temperature differences are large enough. If the pressure change between two columns is insufficient to provide a suitable temperature difference, one of the feasible methods for the heat integration is to use an economizer in the

fresh feeds, which can enable the full use of the high temperature of the recycled solvent (Ghuge *et al.,* 2017). On the other hand, the heat integration and a side-stream withdrawal will increase the complexity of the EDS process and lead to the optimization difficulty. Sequential iterative optimization (Shi *et al.,* 2019; Zhao *et al.,* 2018), SQP solver (Hu *et al.,* 2019; Lang and Biegler, 1987; Yang *et al.,* 2017) and genetic algorithm (GA) methods (Contreras-Zarazúa *et al.,* 2018; Gomez *et al.,* 2010; Mitra and Gopinath, 2004) have been widely applied in the process optimization. The GA method is a global optimization search algorithm, wherein multiple variables are evaluated simultaneously. A set of the Pareto-optimal solutions with multiple conflicting objectives can be obtained through GA to conform to the specified purity constraints. Many researches have exhibited the superiority of GA in the optimization of the chemical intensification processes. For example, Rezende *et al.* (2008) reported the performances of the GA optimization in improving the productivity of 2-methyl-cyclohexanol in the catalytic reactor. With the aim of minimizing the capital and operating cost, Chua *et al.* (2017) employed the multi-objective optimization in designing an energy-efficient reactive distillation process for the isopropyl alcohol production. Su *et al.* (2020) greatly improved the GA optimization to search valuable solutions for stakeholders' preference more purposefully. Moreover, Vazquez–Castillo *et al.* (2009) utilized the GA for the evaluation of multi-objective functions when optimizing the intensified distillation systems. For the separation of the azeotropic mixture of acetonitrile and water by the ED process, the multi-objective optimization using GA method was also verified to be effective, and the solutions of minimizing total cost, energy consumption and separation efficiency was presented by You *et al.* (2018). Nevertheless, there is no published literature applying the GA in the multi-objective optimization for the EDS process of the heat-integration (EDSH). As such, the multi-objective optimization procedure through GA here is utilized to study the process intensification of separating EtAC and EtOH.

Although the optimal EDS process is an attractive structure, few dynamic performances have been investigated to validate the operation feasibility and controbility pratically (Ma, K. *et al.,* 2019; Yang *et al.,* 2019b). Previously, Ma, K. *et al.* (2019) explored the dynamic control of the energy-saving EDS process with composition controllers, yet the control structures of EDS were still worth to be improved. In addition, some common control structures have been developed to

maintain the product purities during the distillation processes. For instance, Yang *et al.* (2019a) proposed an effective control strategy with temperature proportion cascade in the pressure swing distillation for the separation of tetrahydrofuran/ethanol/water mixture. And the control strategies for a reactive distillation involved the double temperature and one-temperature-one-composition structures were fully investigated by Lai *et al.* (2007). Furthermore, Wang *et al.* (2018b) investigated a composition and solvent-to-feed (S/F) proportion control structure for the triple-column side-stream ED process which can handle only 5% feed flowrate disturbances. Inspired by the above dynamic studies, we eventually propose a feasible control strategy for the EDSH process to separate EtAC and EtOH, in which composition proportion cascade is applied to deal with the 10% disturbances of flowrate and composition in the fresh feed.

On the basis of the research of separating azeotropic mixture of EtAC/EtOH through the ED scheme (Zhang *et al.,* 2018), herein the design and control of a proposed energy-efficient EDS with the heat integration is fully studied. A systematic framework of the conceptual design, optimization and control for the separation of EtAC/EtOH is therefore presented. Firstly, an innovative EDS process is proposed to separate such azeotropic systems, Afterwards, the thermodynamic conceptual insight including residue curve maps is conducted to determine the feasible composition regions and the corresponding separation sequences. The proposed process with detailed optimal parameters is then obtained *via* the GA optimization which has exhibited its superiority in evaluating the multiple objectives and obtaining the optimal solution. The total annualized cost and CO_2 emissions are introduced in order to evaluate the economic and environmental performances. Finally, an improved control structure (CS3) with feedforward and composition proportion cascade strategies is established to overcome the instability of the side-withdrawal stream when undergoing the feed flowrate and composition disturbances. In fact, the capability of different control structures rejecting the disturbance in fresh feed flowrate and composition is compared in terms of the offset and transient deviation. The integral absolute error, a quantization valuable, is utilized to directly undergo an assessment on the controllability.

2. Methodology

2.1 Thermodynamic insights on the residue curve maps.

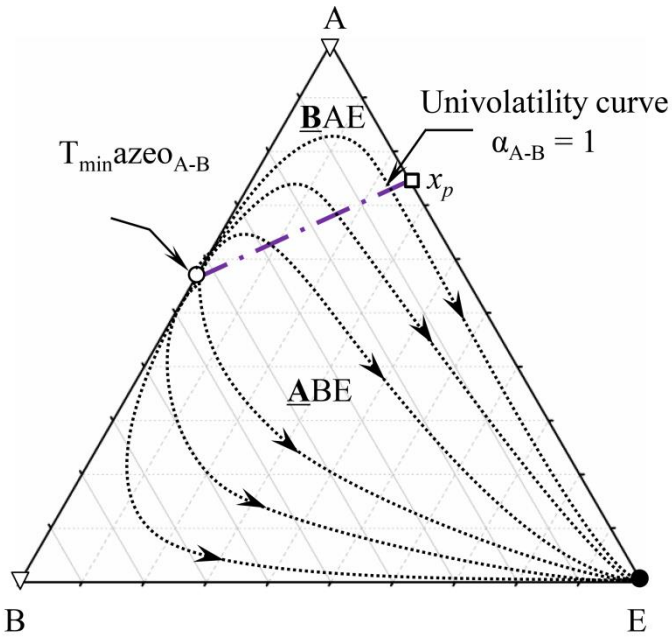

Fig. 1 The residue curve maps of the 1.0-1a class

The binary minimum-boiling azeotrope (*e.g.,* EtAC-EtOH) with heavy entrainer (*e.g.,* DMSO) belongs to the 1.0-1a class of the Serafimov's classification (Kiva et al., 2003)(**Fig. 1**). The binary azeotropic point is an unstable node (*i.e.,* UN_{rcm}) in the residue curve maps (RCMs). Meanwhile, the distilled product components (*i.e.,* A and B) behave as the saddles (*i.e.,* S_{rcm}). And the heavy entrainer (*i.e.,* E) represents a stable node (*i.e.,* SN_{rcm}) of the RCMs. Round dot residue curves (**Fig. 1**) always starts from the UN_{rcm} to the SN_{rcm} following an increasing temperature direction. According to the feasibility criterion of the separation, generally, the univolatility curve (*i.e.,* α_{AB} = 1) always divides the ternary diagram into two regions such as **B**AE and **A**BE (**Fig. 1**). For example, when the ternary mixture is located in the **B**AE region, the pure component B will be the initial distilled product. In addition, the univolatility curve α_{AB} = 1 ends into the binary A-E side and an intersection point x_P can be obtained. The smaller the distance between the x_P point to the separated pure component (*i.e.,* A), the more effective of the entrainer is (Luyben, 2013b). However, there is a minimum flow rate of the employed entrainer for effective separation, and only if the flow rate of the entrainer is larger than that value, the feasible operation by ED can be achieved. Therefore, the optimization solver has to provide the optimal flowrate of entrainer for a

proposed ED scheme.

2.2 Conventional extractive distillation process

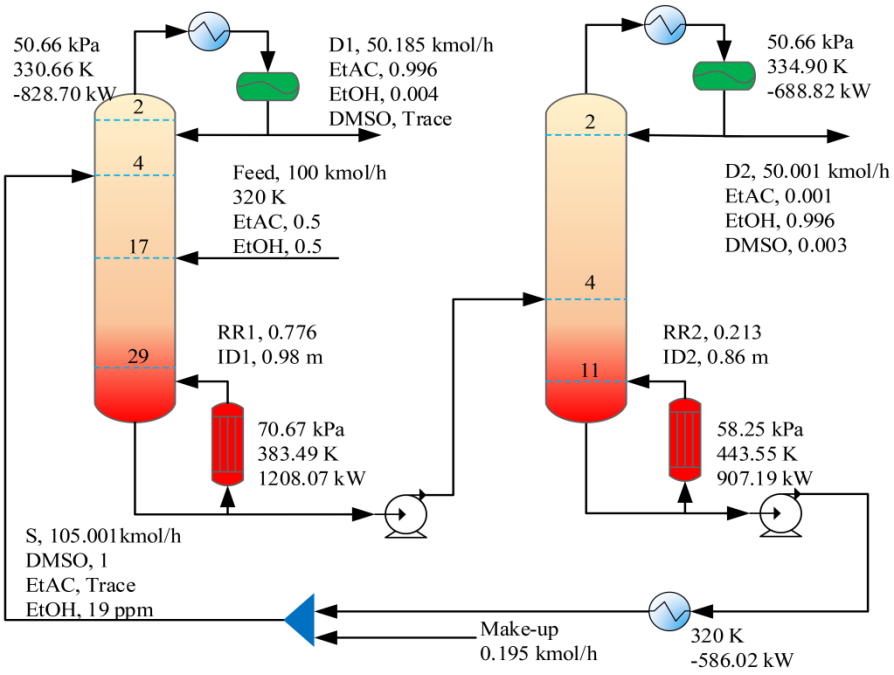

Fig. 2 The conventional ED process for the separation of EtAC/EtOH

During the synthesis process of EtAC by the dehydrogenation of ethanol, the effluent is a mixture of EtAC and EtOH. To achieve the energy-saving separation, the ED process using entrainer dimethyl sulfoxide (DMSO) has been explored by Zhang *et al.* (2018). Because of the large influence of thermodynamic proprieties on the separation process (Su *et al.*, 2019; Wang *et al.*, 2019), the selection of a proper thermodynamic model is also important. On the basis of the existing ED process, the UNIQUAC is used to describe the vapor-liquid phase equilibrium of EtAC-EtOH-DMSO and binary interaction parameters are provided in **Table 1**.

Table 1 The binary interaction parameters of the UNIQUAC model for the EtAC-EtOH-DMSO system

Component i	EtAC	EtAC	EtOH
Component j	EtOH	DMSO	DMSO
Temperature units	K	K	K
Sources	APV-VLE	APV-VLE	APV-VLE
a_{ij}	-0.2733	0.0000	0.0000
a_{ji}	0.6541	0.0000	0.0000
b_{ij} (K)	-159.1655	-200.0622	-13.1028
b_{ji} (K)	-155.2346	35.0858	154.5408

The ED process with optimal detailed parameters for the separation of EtAC/EtOH is demonstrated in **Fig. 2**. The equimolar fresh feed of EtAC and EtOH (totally 100 kmol/h) is introduced into the extractive distillation column (EDC) under the pressure of 50.66 kPa. Of note is that the tray pressure drop of each column is set as 0.69 kPa according to Luyben (2013b). And the high-purity EtAC with 99.6 mol% is obtained on the top of the EDC. Following which, the binary mixture of EtOH and DMSO is separated in the solvent recovery column (SRC), operating at the pressure of 50.66 kPa. An entrainer make-up stream with a certain value of flowrate has to be introduced owing to the loss of DMSO in the distillates. The liquid composition and temperature profile are presented for the optimal ED process in **Fig. A1** in **Appendix A**.

2.3 The proposed side-stream ED process

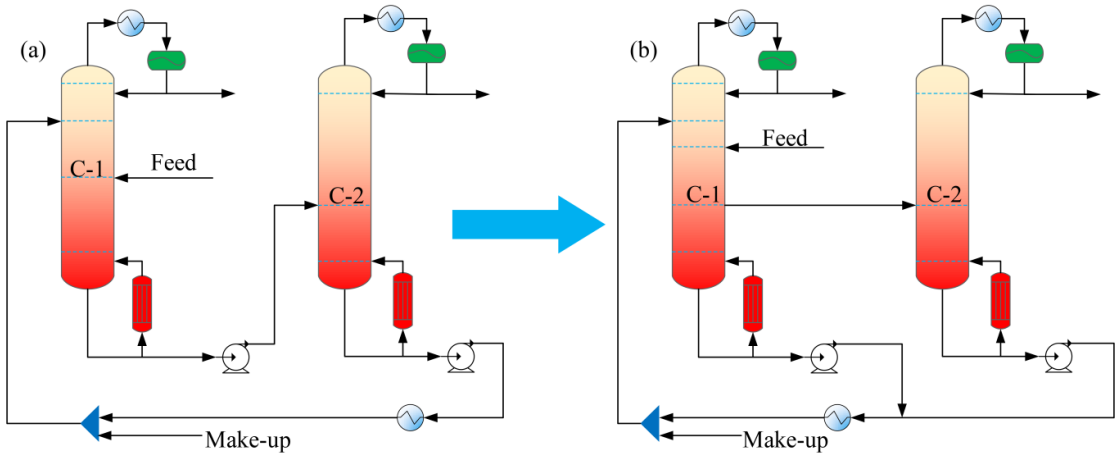

Fig. 3 (a) The conventional ED process; (b) the alternative ED process with side-stream withdrawal for the separation of the minimum-boiling azeotrope mixture

The main objective of this research is to extend the conventional ED to an optimal energy-saving scheme (**Fig. 3**). The C-1 column of the conventional ED scheme is substituted by a side-stream extractive distillation column (SEDC), and the lightest component can be distilled on the top of the column. Furthermore, the C-2 column in **Fig. 3(b)** produces another pure component as the overhead product. The bottom solvent streams from C-1 and C-2 are mixed and recycled to assist in the separation, and the purpose of saving energy can be thus achieved. The operation pressure and the pressure drop in each tray of the EDS are keeping consistent with that in the conventional ED process.

2.4 Process optimization

The optimization process for the EDS system design needs to be implemented in order to find the suitable operating parameters pertaining to the specified constraints (*e.g.,* the purity of products). In comparison with the sequential iterative optimization procedure which has been already applied widely, GA exhibits attractive advantage to conduct a multi-objective optimization meanwhile assessing the influence of different parameters on the solution simultaneously (Bortz et al., 2014).

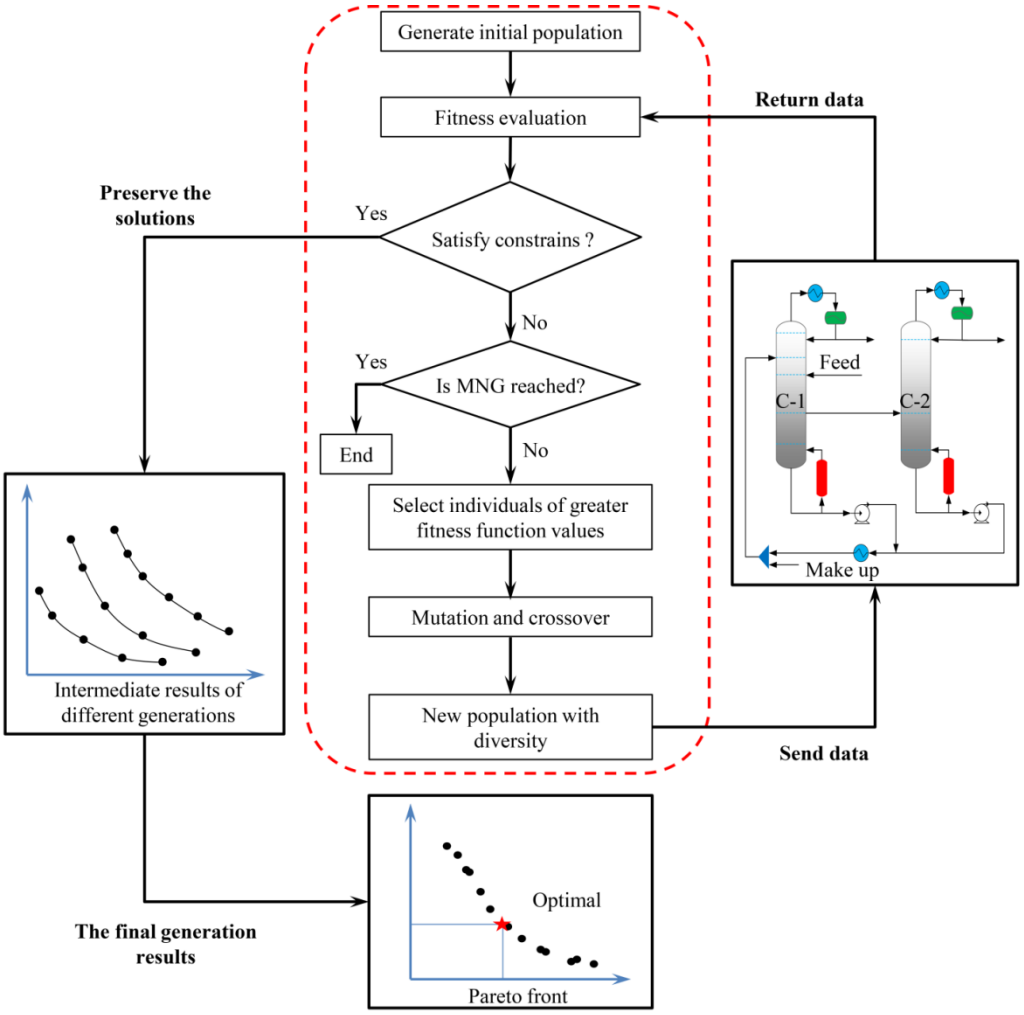

Fig. 4 The genetic optimization procedure with multiple objectives for the ED process

The applied optimization procedure is presented in **Fig. 4**. From the beginning of the design, GA generates the first population of individuals (*i.e.,* the solution of the problem). After that, the fitness function assessment will be conducted to measure the ability surviving in the environment for an individual in the first population. Individuals at the front sequence represent greater values

of the fitness function. Of note is that GA uses the simulation, resulting from professional simulator, to evaluate the corresponding fitness function. The connection between the simulator and the optimization procedure is achieved with the assistance of ActiveX Controls to allow information exchange. Afterwards, those of greater fitness will be selected as the parents of a new generation and the selection process is similar to the biological evolution. Following that, the selected parents are conducted the crossover and mutation to generate diversity of the offspring. Up to now the new generation is generated including the "parents" and "children" individuals. Again, fitness evaluation, selection, mutation and crossover procedure will be performed to continuously preserve the best individuals of each generation. The optimization is implemented until satisfying the cease signal (*e.g.,* the maximum number of generations is achieved). Finally, a set of solutions satisfying the specified constraints with different manipulated variables are obtained. As is evident in **Fig. 4**, the solution points are displayed in the Pareto fronts with multi-objectives. In this research, non-dominated sorting genetic algorithm (NSGA) was employed to obtain the Pareto front which has also been applied to optimizing the ideal Petlyuk sequences (Gutiérrez-Antonio and Briones-Ramírez, 2009). In the final generation, the Pareto optimum solutions exhibit little improvement compared with the previous ten generation solutions. On the basis of the specified practical problem and experience from researchers, one group of design variables is selected. In other words, finding the optimum design in the Pareto front can be explained as finding a good trade-off between conflicting objectives of the practical problem.

The total capital cost (represented by CAP) and the annual operating cost (represented by ENR) are selected as two conflicting objectives, since a higher equipment investment frequently results in more energy savings. Herein, the CAP and ENR are simultaneously minimized by GA optimization, which can be simplified in **eq. (1)**.

$$\begin{aligned} &\textit{Objective function}\begin{cases}\min CAP = f(N_{T1}, N_{F1}, N_{REC}, N_S, F_S, N_{T2}, N_{F2}, D_1, RR_1, D_2, RR_2, REC)\\ \min ENR = f(Q_{R1}, Q_{C1}, Q_{R2}, Q_{C2}, Q_{Cool}, REC)\end{cases}\\ &\textit{Subject to}:\\ &x_{EtAC} \geq 99.6\ mol\%\\ &x_{EtOH} \geq 99.6\ mol\%\\ &x_{REC} \geq 99.9\ mol\% \end{aligned} \tag{1}$$

Where N_{T1} and N_{T2} are the number of column trays, N_S and the F_S are the location of the side-stream and its molar flowrate, and N_{F1}, N_{F2}, N_{REC} represent the feed locations of two feed streams and the recycled solvent, respectively. D_1 and D_2 are molar flowrates of the distillates of SEDC and SRC. RR_1 and RR_2 represent the reflux ratios of SEDC and SRC, REC is the molar flowrate of the recycled solvent. x_{EtAC} is the purity of EtAC at the distilled stream while the purity of EtOH is denoted as x_{EtOH}. The desired purity of the solvent arriving at the SEDC is represented by x_{REC}.

The parameters of the GA are set as 300 individuals. Crossover and mutation factors are set as 0.8 and 0.05, respectively. These parameters were applied based on a similar optimization work in which EDWC process was optimized (Bravo-Bravo et al., 2010). And the overall optimization procedure was carried out on a 64-bit desktop computer with an AMD Ryzen 5 2600 six-core CPU@3.4 GHz, including a 16 GB RAM.

2.5 The economic and CO_2 emissions evaluations

With the implement of the genetic algorithm, TAC is obtained with the aim of taking an economic comparison among different separation schemes. Following the suggestions of Douglas (1988), TAC is defined by **eq. (2)**.

$$TAC = \frac{CAP}{Payback\ period} + ENR \tag{2}$$

Herein, CAP is the total capital cost including the equipment cost of the columns, trays, condensers, reboilers and heat exchangers. However, small items such as reflux drums, pumps, valves and pipes are usually not considered in the calculation due to their much lower costs when comparing to the distillation columns. Moreover, the ENR is the annualized energy cost used by reboilers and condensers, namely, the steam and cooling water cost. Of note is that the steam in different pressure will be applied in the distillation system which depends on the reboiler temperature. Following the suggestions of Luyben (2013b), the payback period is set as three years with the annualized operation time of 8000 hours. And **Table 2** lists the detailed economic calculation on the FORTRAN for the economic evaluation (Olujić et al., 2006; Wang et al., 2018a).

Table 2 The necessary formulas and parameters for economic evaluation

Column diameter (*d*): Aspen Plus tray sizing

Column height (*h*): $h = 0.6096 \times (N_T - 2) \times 1.2$

N_T represents the number of trays

Column and other vessel (*d* and *h* are in meters):

$$\text{capital cost (\$)} = \left(\frac{M\ \&\ S}{280}\right) \times 3919.32 \times d^{1.006} \times h^{0.802}$$

Column Tray (*d* and *h* are in meters):

$$\text{capital cost (\$)} = \left(\frac{M\ \&\ S}{280}\right) \times 97.243 \times d^{1.55} \times h$$

Reboilers (area in m^2):

heat-transfer coefficient = 0.568 kW/K·m^2

differential temperature = steam temperature − base temperature

heat-transfer area: $A_R = \frac{Q_R}{U_R \times \Delta T_R}$

$$\text{capital cost (\$)} = \left(\frac{M\ \&\ S}{280}\right) \times 1775.26 \times A_R^{0.65}$$

Condensers (area in m^2):

heat-transfer coefficient = 0.852 kW/K·m^2

differential temperature = logarithmic mean temperature difference of (inlet and outlet temperature differences)

heat-transfer area: $A_C = \frac{Q_C}{U_C \times \Delta T_C}$

$$\text{capital cost (\$)} = \left(\frac{M\ \&\ S}{280}\right) \times 1609.13 \times A_C^{0.65}$$

Energy cost:

low pressure steam = 7.78 \$/GJ (6 bar, 433 K)

medium pressure steam = 8.22 \$/GJ (11 bar, 457 K)

high pressure steam = 9.88 \$/GJ (42 bar, 527 K)

cooling water = 0.354 \$/GJ (305.15 to 313.15 K)

chilled water = 4.43 \$/GJ (273.15 to 278.15 K)

Marshall & Swift index (*M&S*): 1536.5

It is well-known that the energy consumption during the distillation process has a strong relationship with the CO_2 emission since utility devices in the distillation system are applied to provide heat and steam *via* the fuel combustion. Owing to the necessity of the environment protection, CO_2 emissions for the chemical process should also be applied as an evaluation criterion (Dai et al., 2019; Zhang et al., 2019). A simple model for calculating the CO_2 emissions of the typical industrial process devices such as boilers, furnaces and turbines was introduced by

Gadalla *et al.* (2005). And CO_2 emissions (kg/h) are obtained by **eq. (3)**.

$$[CO_2]_{Emiss} = Q_{Fuel} \times Fuel_{Fact} \quad (3)$$

Where Q_{Fuel} (kJ/h) represents the total heat emission from the fuel combustion in a heating device. And the effect of the fuel can be seen in the terms of $Fuel_{Fact}$ (kg/kJ) which is defined by **eq. (4)**.

$$Fuel_{Fact} = (\frac{\alpha}{NHV})(\frac{C\%}{100}) \quad (4)$$

Where α is 3.67, and NHV (kJ/kg) represents the net heating value of a fuel with carbon content of C%. In general, the values of NHV and $C\%$ of the heavy fuel oil are 39771 kJ/kg and 86.5%, respectively, while the values of NHV and $C\%$ of the natural gas are 51600 kJ/kg and 75.4%, respectively (Gadalla et al., 2005). The steam for heating is produced by the traditional sources such as coal, heavy fuel oil and natural gas. In this research, heavy fuel oil is assumed for providing the steam used in the reboiler (Ma, S. et al., 2019). The Q_{Fuel} (kJ/h)in a furnacecan be calculated by **eq. (5)**.

$$Q_{Fuel} = \frac{Q_{proc}}{\lambda_{proc}}(h_{proc} - 419)\frac{T_{FTB} - T_0}{T_{FTB} - T_{Stack}} \quad (5)$$

Where $\lambda_{proc}(kJ/kg)$ and $h_{proc}(kJ/kg)$ are the latent heat and enthalpy of steam delivered to the process, respectively. Q_{proc} (kJ/h) represents the heat duty of the distillation columns. And T_{FTB}, T_{Stack} and T_0 are the flame temperature of the boiler flue gases, the stack temperature and the ambient temperature, respectively. Generally, the T_{FTB} and T_{Stack} are assumed as 2073.15 K and 433.15 K, while T_0 is set as 298.15 K (Yang *et al.*, 2019c).

2.6 Dynamic control

One of the most important tasks is to explore the dynamic control schemes for the industrial application of the energy-saving configuration for separating such azeotropic system. For the implementation of the dynamic design, firstly pumps and valves with specified phase settings are installed to take a pressure checker. Herein, pumps and valves are expected to provide proper pressure drops of 300 kPa to deal with the feed disturbances without leading to the valve saturation (Yang et al., 2019c). The volumes of reflux drums and sumps are specified to give 5 min holdup with 50% liquid level. After that, the steady-state model is exported to the dynamic

simulation using pressure-driven settings. Following which, step disturbances of feed flowrate and composition are introduced to test the process controllability. To ensure operation safety, several control variables such as feed flowrates, liquid levels and pressure have to be maintained at or close to their set points. The product purity is indicated by the specified tray temperature since the composition variation on each tray depends on the corresponding tray temperature under specified pressure.

Foremost, open-loop sensitivity analysis is applied in determining the suitable temperature-sensitive stage (Pan et al., 2019). Novel temperature distributions of column trays can be obtained after a very small fluctuation (*i.e.,* 0.1%) of manipulated variables (*e.g.,* reflux flowrate and reboiler duty) is introduced meanwhile other manipulated variables are retained at nominal values (Luyben, 2017). Therefore, the steady-state gain matrix **K** with respect to the manipulated variable can be attained by the proportion of the temperature fluctuation amplitude in different trays to the corresponding fluctuation amplitude of the manipulated variable (**eq. (6)**). Singular value decomposition (SVD) is an effective method to select control pairs when the different manipulated variables shows the same temperature-sensitive plates. According to the **eq. (7)**, the corresponding plate of the maximum value of each column in the **U** matrix is the sensitive plate, and the corresponding manipulated variable is the control object to be paired.

$$K = \Delta C_V / \Delta M_V \tag{6}$$

$$K = U \sum V^T \tag{7}$$

Where $\mathbf{\Delta C_V}$ is the changes in stage temperatures, $\mathbf{\Delta M_V}$ is the step change in manipulated variables. **K** represents the steady-state gain matrix, **U** and **V** are the orthonormal matrices and $\sum$ is a diagonal matrix of singular values.

The maximum transient deviation and oscillation amplitude are the main considerations for evaluating the distillation control system, which directly affects the integral absolute error (IAE) value. In general, the larger IAE value stands for the worse dynamic performance. The IAE defined in **eq. (8)** is used as the quantitative criterion to evaluate the dynamic performance of

different control structures.

$$\mathrm{IAE} = \int_0^T \mid e(t) \mid dt \tag{8}$$

Where ***e*** represents the deviation of the manipulated variable from the desired set point and ***T*** is the dynamic simulation time.

3. Analysis and optimization results

3.1 Thermodynamic insights of ternary system of EtAC/EtOH/DMSO

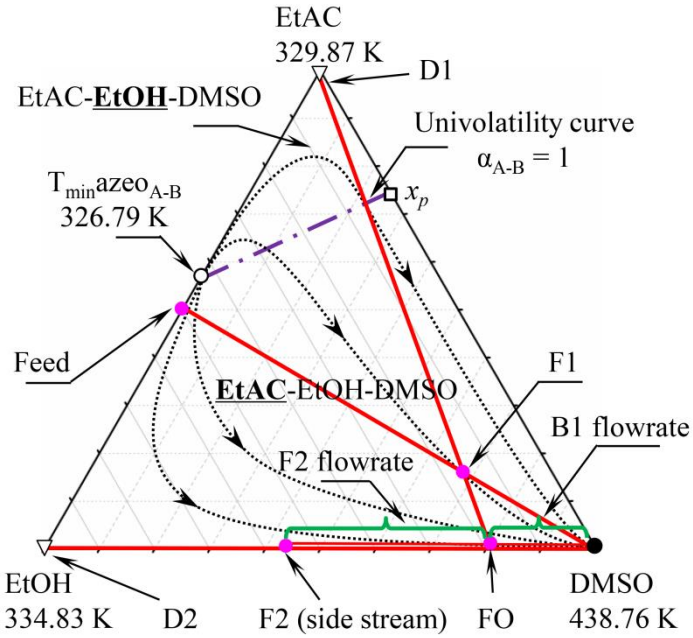

Fig. 5 The thermodynamic insights of separating EtAC/EtOH with entrainer DMSO by the EDS scheme

The residue curves and material balance lines (represented by red lines) for the proposed EDS scheme of separating EtAC and EtOH at 50.66 kPa are illustrated in **Fig. 5**. Heaviest entrainer DMSO is the stable node (SN_{rcm}) with a boiling point at 438.76 K, and the binary azeotrope of EtAC/EtOH is an unstable node (UN_{rcm}) with 326.79 K. Moreover, the EtAC and EtOH are saddles (S_{rcm}) and their boiling points are 334.83 K and 438.76 K, respectively. The univolatility curve divides the ternary diagram into two different regions, and the feed mixture at the lower region (*i.e., **EtAC**−EtOH−DMSO*) will be separated to obtain EtAC initially. From the analysis of the material balance lines, some conclusions of the conceptual design for the separation can be drawn as follows: a) the fresh feed point (*i.e., Feed*) is mixed with the entrainer stream of DMSO

to obtain a mixture input (*i.e., F1*) in the first column SEDC; b) the "*F1*" mixture can be separated into the distilled stream with high-purity EtAC and another stream "*FO*" according to the material lines; c) a side-stream product represented as "*F2*" and the bottom entrainer stream "*B1*" are further achieved from the "*FO*" in the first column; d) the side stream "*F2*" is introduced into the SRC to attain EtOH with 99.6 mol% on the top. Both entrainers from the bottom of two columns are mixed and further recycled to the SEDC.

3.2 The degree of freedom

The proposed EDS system involves two columns (*i.e.,* the SEDC and SRC) which have different degrees of freedom.

For the SEDC, the operation pressure and the fresh feed condition are fixed. Meanwhile, the other parameters such as the total number of stages (N_{T1}), the locations of the fresh feed (N_{F1}) and recycled entrainer (N_{FE}), the molar flowrate of the distillate (D_1) and the reflux ratio (RR_1) are optimized variables. And the flowrate of the recycled entrainer (*REC*) is added as the optimization variable while the temperature of the recycled solvent is fixed at the 320K to retain consistent with the conventional ED process. In addition, the SEDC has another liquid side stream, which results in two extra degrees of freedom. The location of the side stream (N_S) and the flowrate (F_S) are selected as the optimized variables. In summary, there are eight degrees of the freedom for the SEDC.

Similarly, the SRC has four degrees of freedom with the fixed pressure. And the selected four optimization variables are the total number of stages (N_{T2}), the feed location (N_{F2}), the flowrate of the distillate (D_2) and the reflux ratio (RR_2). The degree of freedom of the EDS system without heat integration is summarized in **Table 3**. During the optimization of the heat-integration scheme (*i.e.,* the EDSH process), the fresh feed is heated to a temperature (*i.e., Temp*) that should also be optimized to obtain the optimal EDSH process. Compared with the EDS process, the EDSH has thirteen degrees of freedom (**Table 3**).

Table 3 The optimization variables of the proposed EDS and EDSH processes

Process		Optimization variables	Degrees of freedom
EDS	SEDC	D_1, RR_1, F_S, N_{T1}, N_{F1}, N_{FE}, N_S, *REC*	8
	SRC	D_2, RR_2, N_{T2}, N_{F2}	4

	Total	12	12
EDSH	SEDC	D_1, RR_1, F_S, N_{T1}, N_{F1}, N_{FE}, N_S, *REC*, *Temp*	9
	SRC	D_2, RR_2, N_{T2}, N_{F2}	4
	Total	13	13

3.3 Optimal process for EDS without heat integration

From the analysis of the degree of the freedom, twelve variables are simultaneously optimized during the EDS process. It lasts three days to obtain the optimal results, with an average of 7 minutes for each generation. The optimization provides a set of design variables meeting the purity constraints in different generations. For instance, the results of multi-objective genetic optimization progression at different generations are plotted in **Fig. 6(a)**. Very limited improvement of the objective functions (*i.e.,* CAP and ENR) can be observed from 200th to 300th generation, thereby the optimization procedure should be terminated after 200 generations. Overall, the Pareto-optimal front of 300th generation obtained from the multi-objective optimization with remained 53 individuals (**Fig. 6(b)**).

To determine the optimal parameters, three data points are considered as the candidate solutions inspired by the research from Alcocer-García *et al.* (2019). **Table 4** demonstrates the detailed parameters of three specified parameters. The three designs are related to the increasing capital investments while reducing energy costs. In comparison with "Data1", it can be observed that the scheme "Data2" presents 2.4% ENR savings and increases 1.9% CAP. On the other hand, the scheme "Data3" presents 3.5% ENR savings when comparing to Data1 with a large increase (7.8%) in CAP. Therefore, the "Data2" exhibits relatively good compromise between two conflicting objectives to minimize the TAC (Alcocer-García *et al.* 2019). Through the optimization of the EDS, the optimal process flowsheet with detailed parameters is demonstrated in **Fig. 7**. The effect of other relative design parameters versus TAC derived from the Pareto front is indicated in **Fig. A2**. In addition, the liquid composition and temperature profile are presented for the optimal EDS process in **Fig. A3** in **Appendix A**.

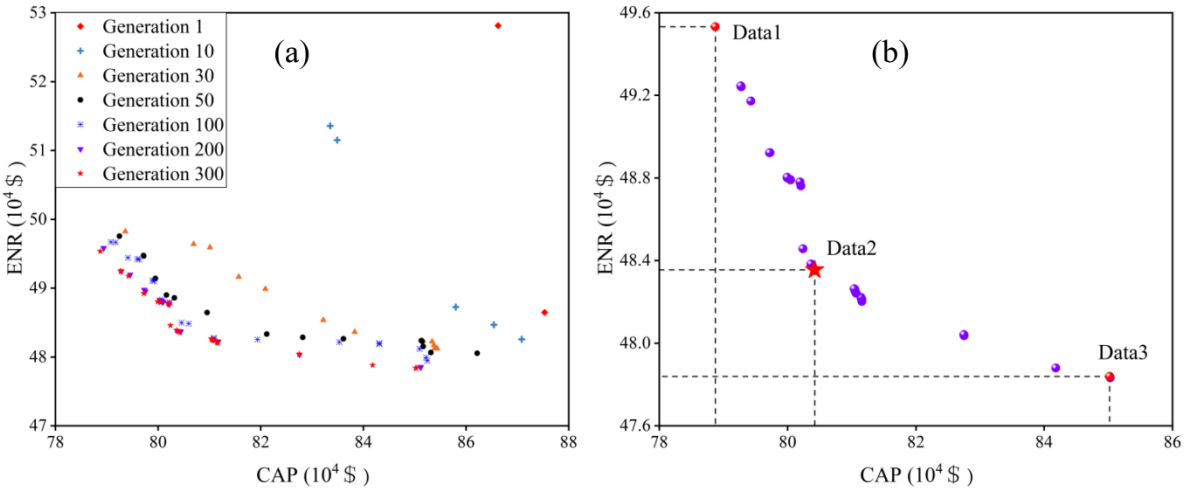

Fig. 6 (a) The GA optimization progression results at different generations; **(b)** Pareto-optimal front of the EDS for 53 individuals and MNG of 300

Table 4 The design parameters and performance indexes for the EDS without heat integration

Parameters	Data1	Data2	Data3
N_{T1}	29	32	38
N_{F1}	10	17	20
N_{REC}	4	5	4
N_{T2}	10	10	10
N_{F2}	5	4	5
N_S	25	28	34
ID_1 (m)	0.980	0.981	0.985
ID_2 (m)	0.756	0.752	0.742
RR_1	0.75	0.797	0.846
RR_2	0.095	0.084	0.084
REC (kmol/h)	116.690	103.937	95.052
F_S (kmol/h)	94.240	91.983	89.275
Q_{C1} (kW)	-818.455	-839.149	-861.842
Q_{R1} (kW)	1345.581	1308.760	1300.353
Q_{C2} (kW)	-614.597	-609.787	-608.166
Q_{R2} (kW)	728.480	715.770	702.594
Q_{cool} (kW)	-624.913	-544.667	-516.818
CAP ($)	788749.243	804250.338	850312.728
ENR ($/y)	495322.617	483547.890	478317.102

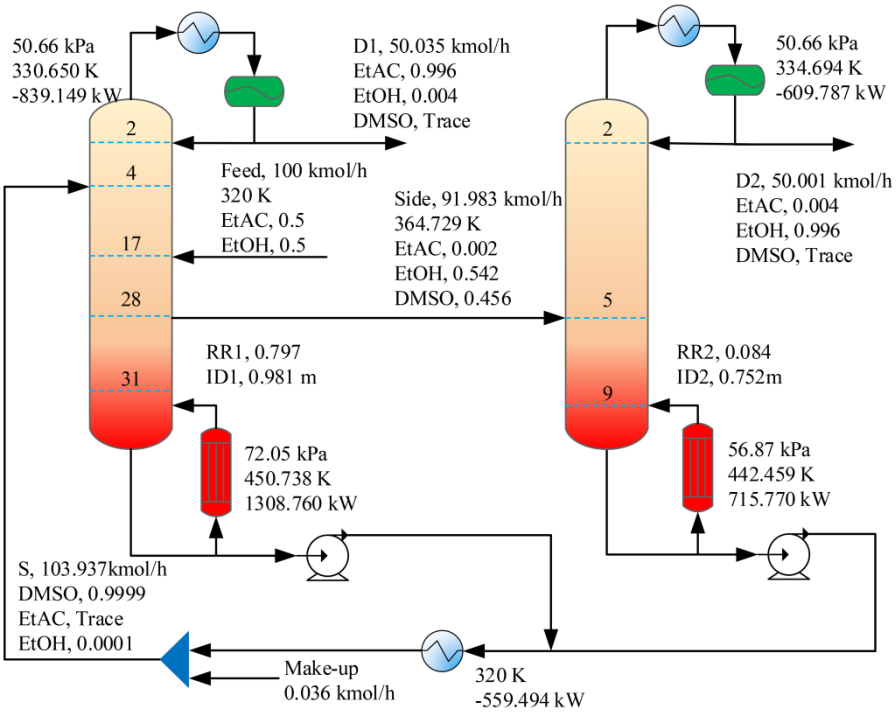

Fig. 7 The EDS scheme with optimal parameters for separating EtAC/EtOH

3.4 Optimal process for EDS with heat integration

To further reduce energy cost, the EDS process with heat integration (EDSH) is investigated according to the basic flowsheet (**Fig. 7**). Herein, instead of utilizing the temperature difference between the condenser and reboiler by changing the pressure, a simple stream-effluent heat integration method is employed owing to the large temperature difference between recycled solvent stream and fresh feed. Similarly, the heat-integrated process should be optimized again and the Wegstein method is also applied to ensure the convergent of the process. The economizer is used for heat transferring without any temperature crossover problem. Since the temperature of recycled solvent does not return to the initial temperature (320 K) after the heat integration, an auxiliary cooler is still needed (**Fig. 9**).

Different from the EDS process, it spends about four days to complete the optimization with an average of 10 minutes for each generation. This is much longer than that for EDS without heat integration since the process becomes more complex. Ultimately, the results of intermediate multi-objective optimization by GA and the Pareto front of 200th generation are given in **Fig. 8**. Three data points are also considered as the candidate solutions similar as **Section 3.2**. And the detailed parameters of three designs are listed in **Table 5**. When compared to the most polluting

design (*i.e.,* "Data1"), the "Data2" presents 4.8% ENR savings and 1.9% increase in the CAP. Relatively, the scheme "Data3" presents 7.5% ENR savings compared to "Data1" with a large increase (4.4%) in the CAP. The optimal solution (*i.e.,* "Data3") shows the lowest TAC (0.7261 million$/year), represented by a red pentacle in **Fig. 8(b)**, and is eventually selected. Indeed, optimization results for some other manipulated variables, namely, number of column stages, feed locations and reflux ratios, are exhibited in **Fig. A4.** Also, the liquid composition and temperature profile are presented for the optimal EDSH in **Fig. A5** in **Appendix A**. Through the optimization of EDSH, the optimal process with heat-integration is illustrated in **Fig. 9**.

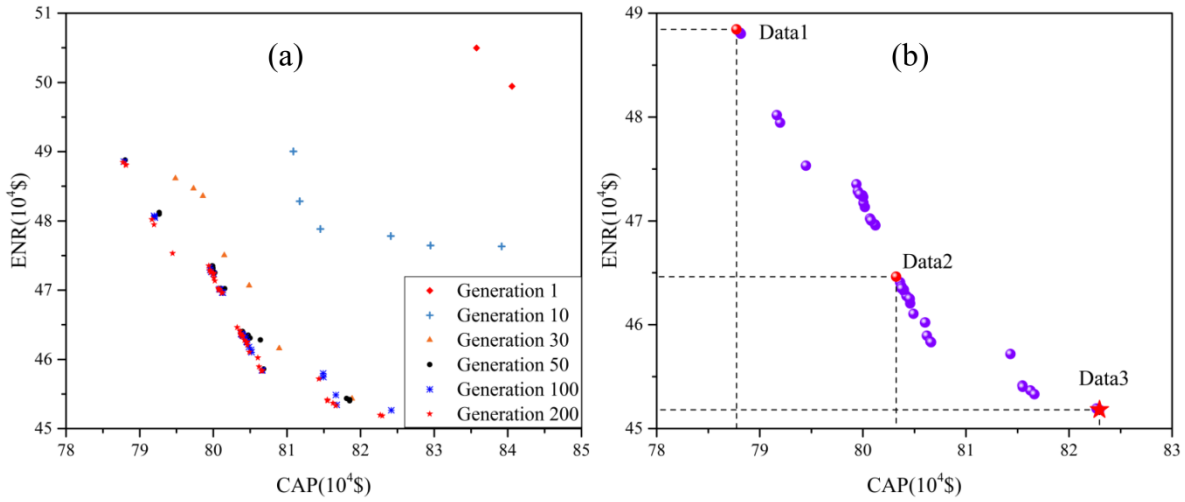

Fig. 8 (a) The GA optimization progression results at different generations for the EDSH scheme; **(b)** Pareto-optimal front of the EDSH for 97 individuals and MNG of 200

Table 5. The design parameters and performance indexes for EDS with heat integration

Parameters	Data1	Data2	Data3
N_{T1}	29	32	32
N_{F1}	16	17	17
N_{REC}	4	4	4
N_{T2}	10	10	11
N_{F2}	6	6	6
N_S	25	27	27
ID_1 (m)	0.984	0.996	1.020
ID_2 (m)	0.760	0.749	0.757
RR_1	0.747	0.799	0.965
RR_2	0.108	0.100	0.095
Temp (K)	331.795	342.998	345.001

REC (kmol/h)	120.080	120.008	103.533
F_S (kmol/h)	98.180	97.545	95.0356
Q_{C1} (kW)	-815.595	-839.901	-917.025
Q_{R1} (kW)	1299.909	1208.978	1160.606
Q_{C2} (kW)	-621.583	-617.497	-613.634
Q_{R2} (kW)	742.466	733.932	727.843
Q_{cool} (kW)	589.102	469.412	341.700
CAP ($)	787685.816	803241.722	822956.920
ENR ($/y)	488063.834	464613.776	451817.024

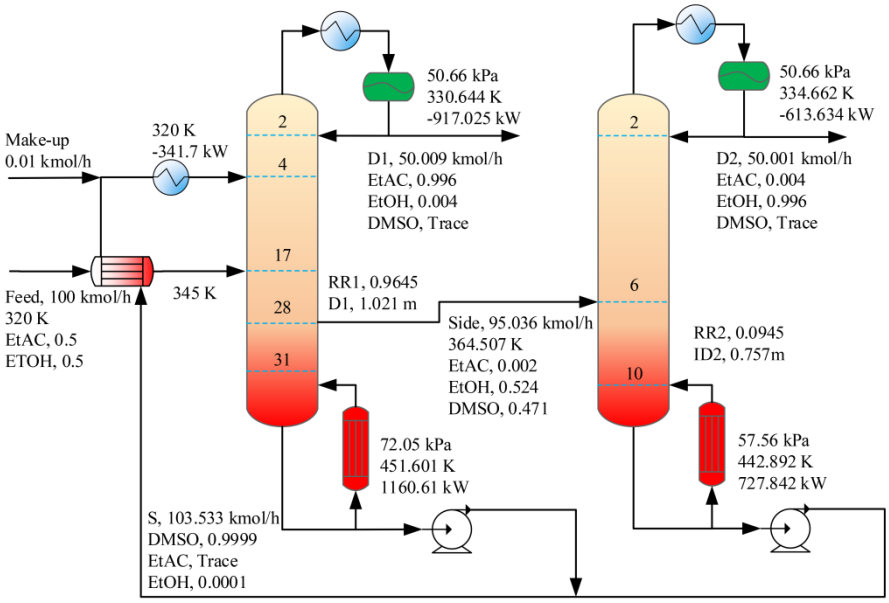

Fig. 9 The EDSH scheme with optimal parameters for separating EtAC/EtOH

3.5 Economic and CO_2 emissions evaluation

In this section, detailed comparisons of the economic performance and CO_2 emission of the conventional ED, EDS and EDSH processes are listed in **Table 6**. In comparison with the conventional ED process, energy consumption in the reboilers of EDS and EDSH are decreased by 4.28 and 10.72%, respectively. Besides, the total capital cost of EDS and EDSH decreases by 5.95% and 3.77%. The reason for decreased energy consumption in the EDS system is that the repeated separation section is reduced after introducing a side stream, which has also been demonstrated in **Fig. A6** in the **Appendix A**. Above all, the proposed EDSH process is the most economical (7.78% savings of TAC) among the three schemes. Besides, the EDSH for the EtAC/EtOH separation has a 9.28% reduction for greenhouse gas CO_2 emissions than the

traditional ED process.

Table 6 The results of the detailed parameters of the TAC and CO_2 emissions for three processes

Separation process	ED	EDS	EDSH
N_{T1}	30	32	32
N_{F1}	17	17	17
N_{REC}	4	5	4
N_{T2}	12	10	11
NF2	4	4	6
NS	-	28	27
ID_1 (m)	0.98	0.98	1.02
ID_2 (m)	0.86	0.75	0.76
Feed Temperature (K)	320	320	345
REC (kmol/h)	105.0	103.9	103.5
F_S (kmol/h)	-	91.98	95.04
Q_{C1} (kW)	-828.696	-839.149	-917.025
Q_{R1} (kW)	1208.070	1308.760	1160.606
Q_{C2} (kW)	-688.823	-609.787	-613.634
Q_{R2} (kW)	907.188	715.770	727.843
Q_{cool} (kW)	-586.020	-544.666	-341.700
Total reboiler duty (kW)	2115.258	2024.530	1888.449
Total condenser duty (kW)	-2103.539	-1993.602	1872.359
CAP ($)	855210.786	804250.338	822956.920
ENR ($/y)	502308.342	483547.890	451817.024
TAC ($/y)	787378.604	751631.336	726135.998
Saving (%)	**0.00**	**4.54**	**7.78**
CO_2 emissions (t/h)	723.845	703.982	656.663
Saving (%)	**0.00**	**2.74**	**9.28**

4. Dynamic control for EDSH process

4.1 Selection of temperature-sensitive trays

According to the evaluation results of economic and environment for the separation of EtAC/EtOH, the EDSH exhibits economic benefits as well as lower CO_2 emissions. However, the less robust dynamic behaviors of EDSH are the undesirable side effects due to the instability of introduced side-stream flowrates. As a consequence, the detailed control structures of the EDSH

process should be further investigated. The molar purity of EtAC and EtOH are 99.62 mol% and 99.64 mol% in the dynamic initialization, respectively. It is noteworthy that the exported dynamic results of products purity obtained are slightly different from the steady-state process. However, it has no influence for the research of the controllability.

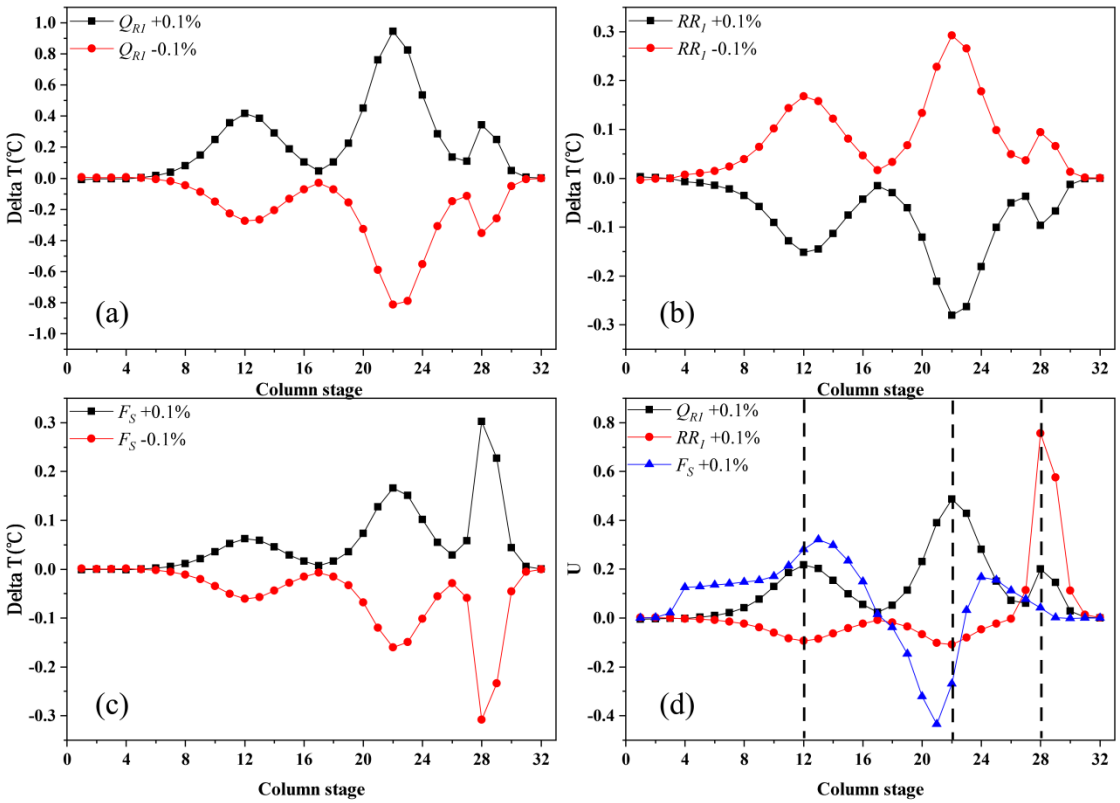

Fig. 10 The open-loop sensitivity plots for ±0.1% changes in manipulated variables (a) reboiler duty; (b) reflux ratio; (c) side-stream flowrate for the tray temperatures of SEDC; and (d) SVD analysis

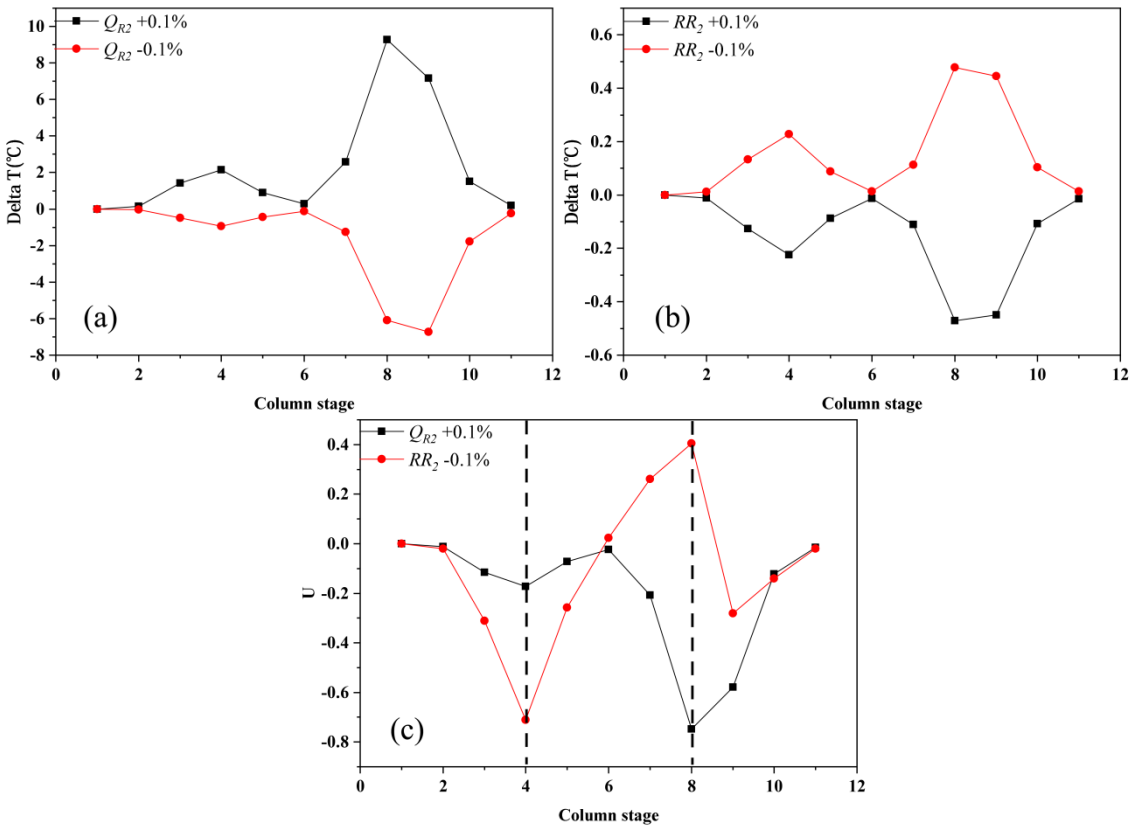

Fig. 11 The open-loop sensitivity plots for ±0.1% changes in manipulated variables (a) reboiler duty; (b) reflux ratio for the tray temperatures of SRC; and (c) SVD analysis

Plots **(a)**, **(b)** and **(c)** in **Fig. 10** demonstrate the sensitivity analysis when undergoing ±0.1% step changes of the SEDC in reboiler duty (Q_{R1}), reflux ratio (RR_1) and side-stream flowrate (F_S). Wherein, there are similar plates (*i.e.,* 12th, 22th and 28th stages) which are all sensitive to the changes in three manipulated variables. **Fig. 10(d)** illustrates the SVD results for the step changes in Q_{R1}, RR_1 and F_S. The temperature of 22th tray (T22) in SEDC has the largest U vector for the change in Q_{R1}. Therefore, T22 should be determined to control the purity of EtAC by adjusting Q_{R1}. The temperature of 28th stage (T28) is not controlled exactly since the side stream is withdrawn at 28th stage. In other words, the flowrate fluctuation of the side stream dramatically affects the stability of the control system. Furthermore, the temperature of the 12th stage (T12) of the SEDC displays an impressive U vector for the changes of RR_1 and F_S, indicating that the T12 could be selected to manipulate the RR_1 or F_S. To determine the suitable manipulated variable, the singular values (*i.e.,* σ) of the steady-state gain matrix are obtained. For instance, $\sigma1 = 2.05$, $\sigma2 = 0.29$ and $\sigma3 = 0.067$ are corresponding to the manipulated variables Q_{R1}, RR_1, and F_S, respectively. According to the suggestions by Luyben (2006), the condition number CN1 = $\sigma1/\sigma2$ = 7.07

indicates that the two selected sensitive tray temperatures (*i.e.,* T22 and T12) are independent by manipulating variables Q_{R1} and RR_1. Comparatively, the condition number CN2 = $\sigma 1/\sigma 3$ = 30.59 implies that T22 and T12 are not suitable by adjusting the variables Q_{R1} and the side-stream flowrate simultaneously. Above all, it is feasible to apply the dual-temperature control scheme to the SEDC. As is evident in **Fig. 11(a)-(b)**, there are two temperature-sensitive stages which are the 4th and the 8th stage, respectively. **Fig. 11(c)** provides the results of SVD analysis for Q_{R2} and RR_2. The temperature of the 8th stage (T8) has the largest change in Q_{R2}, as such T8 should be determined as the controlled variable. Similarly, T4 can be applied to manipulate the RR_2.

4.2 Basic temperature control structure (CS1)

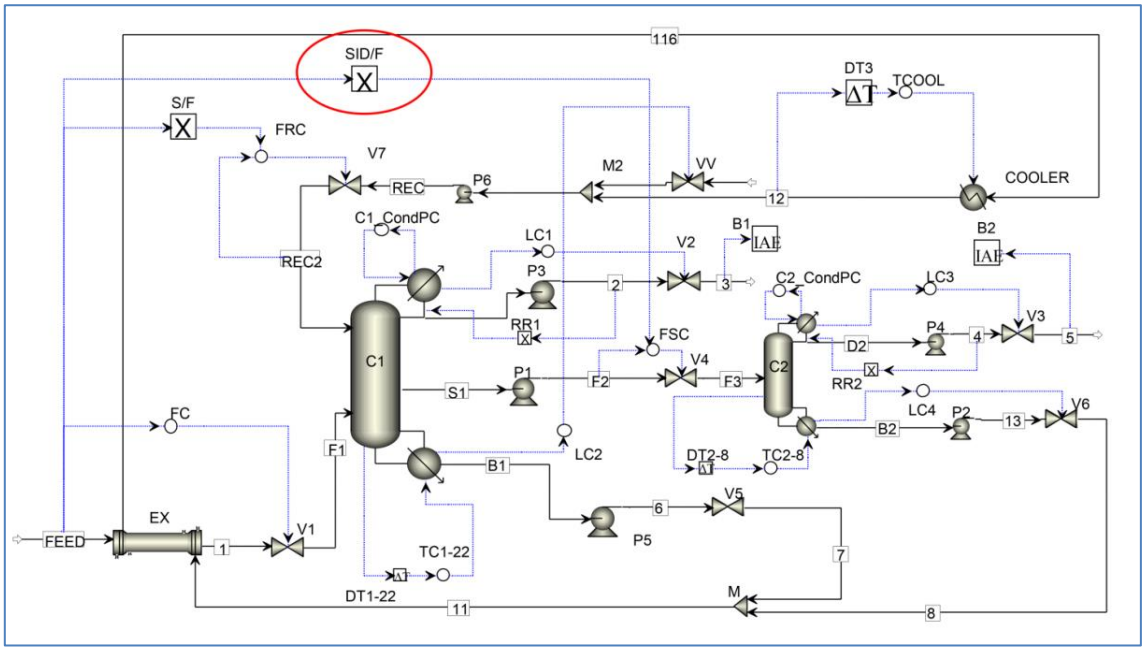

Fig. 12 The basic temperature control structure of the EDSH scheme

Initially, a basic temperature control structure (CS1) of the EDSH is exhibited in **Fig. 12**. To ensure the process safety and obtain the specified product with high purity, several controllers are added in the CS1. And overall detailed control loops and the related settings are illustrated as below:

(1) The fresh feed flowrate is controlled by a throughput valve (reverse acting).

(2) The recycled solvent flowrate is rationed to the total feed flowrate and controlled by a throughput valve (reverse acting).

(3) The side-stream flowrate is rationed to the total feed flowrate and controlled by a throughput

valve (reverse acting).

(4) The operating pressures in two columns are controlled by manipulating the corresponding condenser duties (reverse acting).

(5) The distilled flow rates of two columns are adjusted to control the reflux tank levels (direct acting).

(6) The bottom flowrate of SRC is manipulated to deal with the sump level of the column (direct acting).

(7) The adjustment of entrainer makeup flowrate is to hold the sump level of the SEDC (reverse acting).

(8) The heat exchanger is used to control the temperature of the recycling solvent (reverse acting).

(9) T28 in SEDC and T8 in SRC are respectively controlled by changing the reboiler heat duty (reverse acting).

(10) The reflux ratios in two columns are fixed.

As for the tuning process of temperature controllers, the relay-feedback tests are run with 1 min dead time of temperature controllers, before the Tyreus–Luyben tuning rule is applied to determine parameters of PI controllers. Ultimate gains and integral time of three temperature controllers are listed in **Table 7**.

Table 7 The tuning parameters of the temperature controllers in the CS1

Controllers	**TC1-22**	**TC2-8**	**TCOOL**
Controller action	Reverse	Reverse	Reverse
Manipulated variable	Q_{R1}	Q_{R2}	Q_{cool}
Transmitter range (℃)	0-160.88	0-232.40	0-93.69
Output range (GJ/h)	0-8.84	0-5.23	-3.21-0
Gain K_C	2.06	1.41	0.17
Integral time τ_I (min)	10.56	13.20	5.28

Fig. 13 demonstrates the dynamic performances in the EDSH scheme when the process subjected to ±10% changes in the flowrate and the feed composition. It can be found that CS1 with single temperature control has no capability to guarantee the product purities to achieve the desired values at new steady state when feed composition disturbances are introduced. In the condition of the feed composition changes, the side-stream flowrate could not be properly

adjusted in time. Therefore, the composition disturbance in CS1 is more difficult to be solved when comparing to the feed flowrate disturbance. Especially, when the EDSH system undergoing the changes of decreased feed composition (45 mol% EtAC), the purity offset for the purity of EtAC is not acceptable (**Fig. 13(c)**). In addition, considering that the amount of required reflux flowrate in the SEDC should be changed once feed stream with 45 mol% EtAC is introduced, the reflux ratio of the SEDC cannot be fixed. Therefore, improved control schemes with adjusted reflux ratio should be further explored in order to enable the effective control.

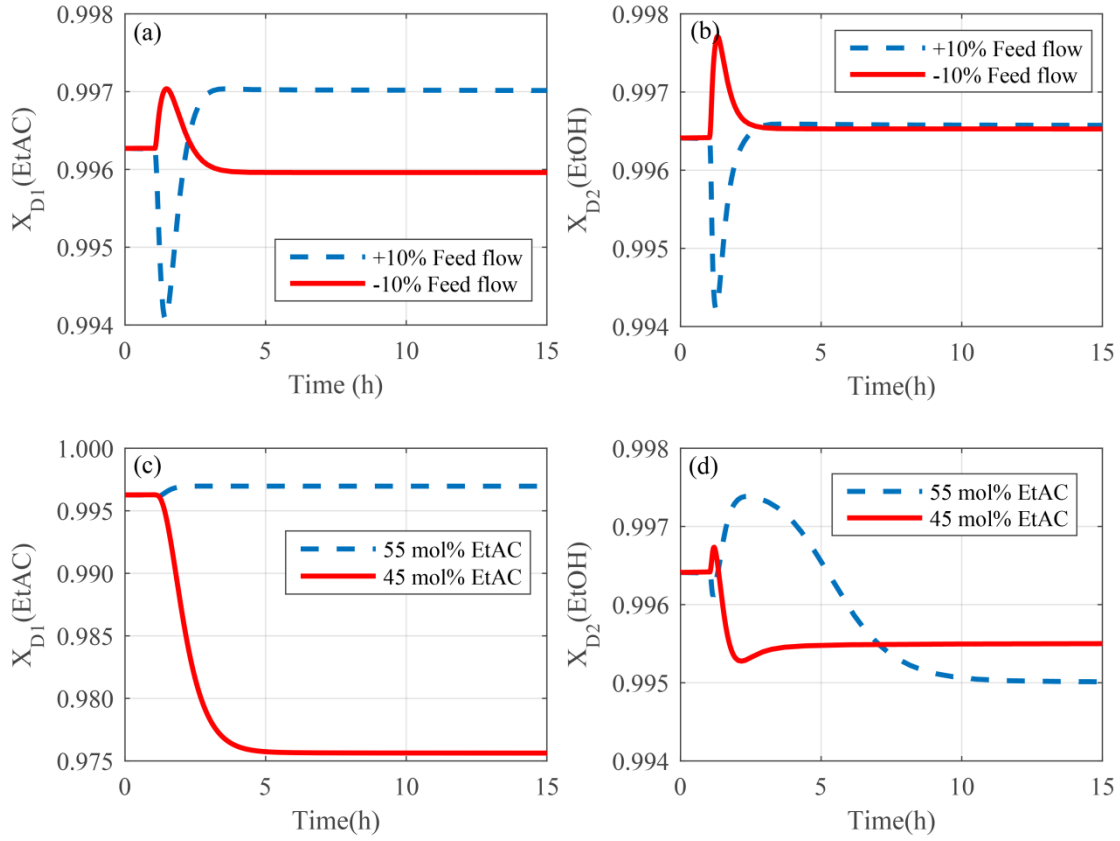

Fig. 13 The dynamic responses for the CS1 under the disturbance of ±10% feed flowrate and ±10% feed composition

4.3 The dual temperature control structure (CS2)

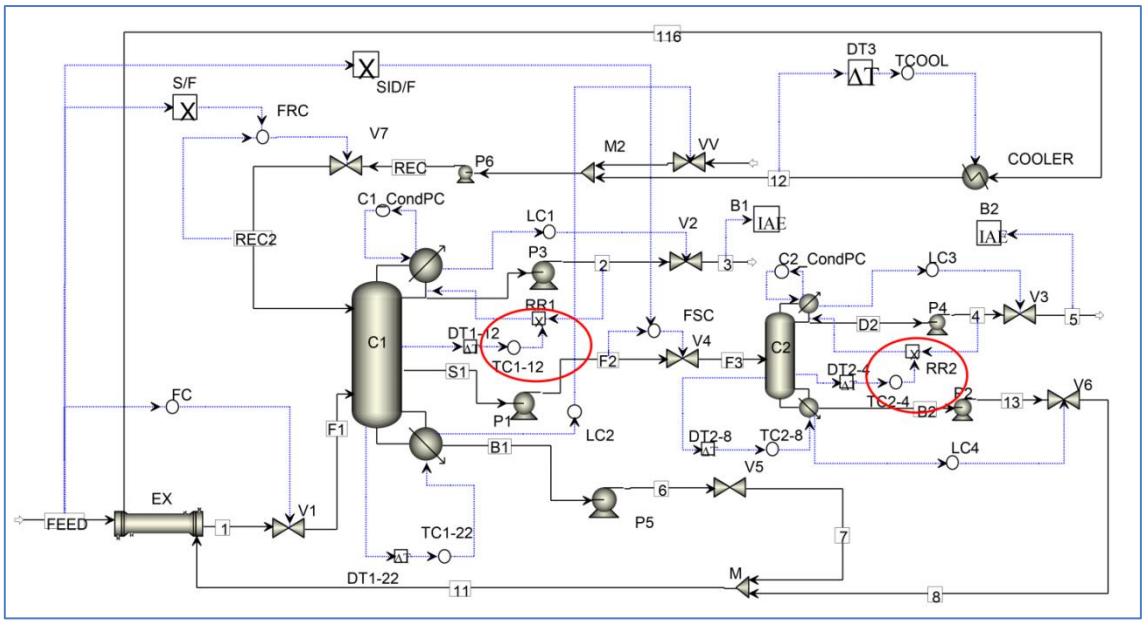

Fig. 14 The improved dual-temperature control structure of the EDSH

On the basis of the open-loop sensitivity analysis for both columns in **Section 4.1**, T12 can be applied to manipulate the reflux ratio of SEDC and T4 is used to adjust the reflux ratio of SRC. Consequently, an improved dual-temperature control structure (CS2) is further investigated (see **Fig. 14)**. Additionally, the tuning parameters of the dual temperature control structure are summarized in **Table 8**.

Table 8 The tuning parameters of the temperature controllers in the CS2

Controllers	TC1-22	TC1-12	TC2-8	TC2-4	TCOOL
Controller action	Reverse	Reverse	Reverse	Reverse	Reverse
Manipulated variable	Q_{R1}	RR_1	Q_{R2}	RR_2	Q_{cool}
Transmitter range (℃)	0-160.88	0-167.26	0-232.40	0-153.79	0-93.69
Output range (GJ/h)	0-8.84	0-1.79	0-5.23	0-0.19	-3.21-0
Gain Kc	2.40	1.33	1.41	55.69	0.17
Integral time τ_I (min)	9.24	19.79	14.52	21.12	5.28

Fig. 15 gives the dynamic responses of the CS2 for the EDSH process after introducing the feed flowrate as well as the composition disturbances. Compared to the CS1, the CS2 enables a better performance in overcoming two feed disturbances. Nevertheless, the processes still have a large offset in the condition of decreasing composition. Although the reflux ratios of two columns have been modified by the corresponding temperatures, the target of controlling the side stream

flowrate has not been directly attained. An inference is that adjusting reflux ratio of SEDC may not be helpful enough for improving the purity of EtAC (**Fig. 15(c)**) under the condition of the feed composition disturbance. In this case, the dynamic performance of the composition disturbances still needs to be improved. As a consequence, a robust control structure with composition controllers should be considered.

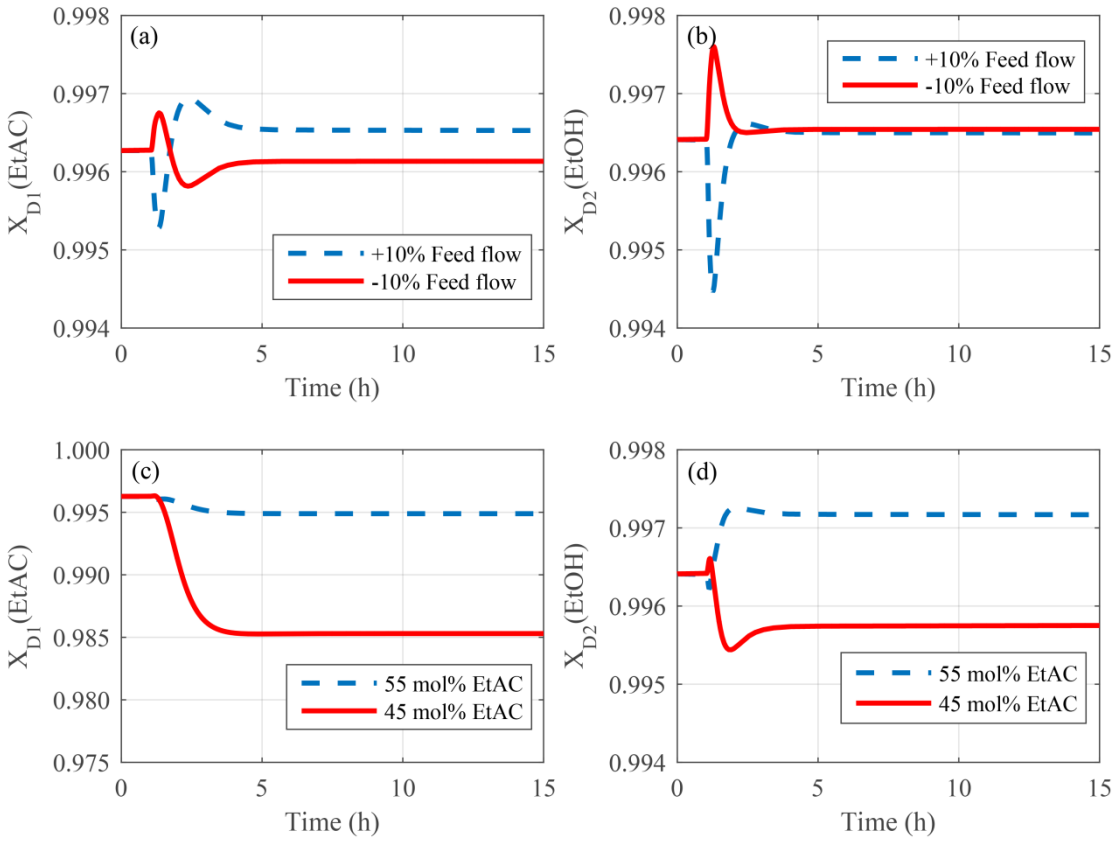

Fig. 15 The dynamic responses for the CS2 under the disturbance of ±10% feed flowrate and ±10% feed composition.

4.4 The improved control structure (CS3)

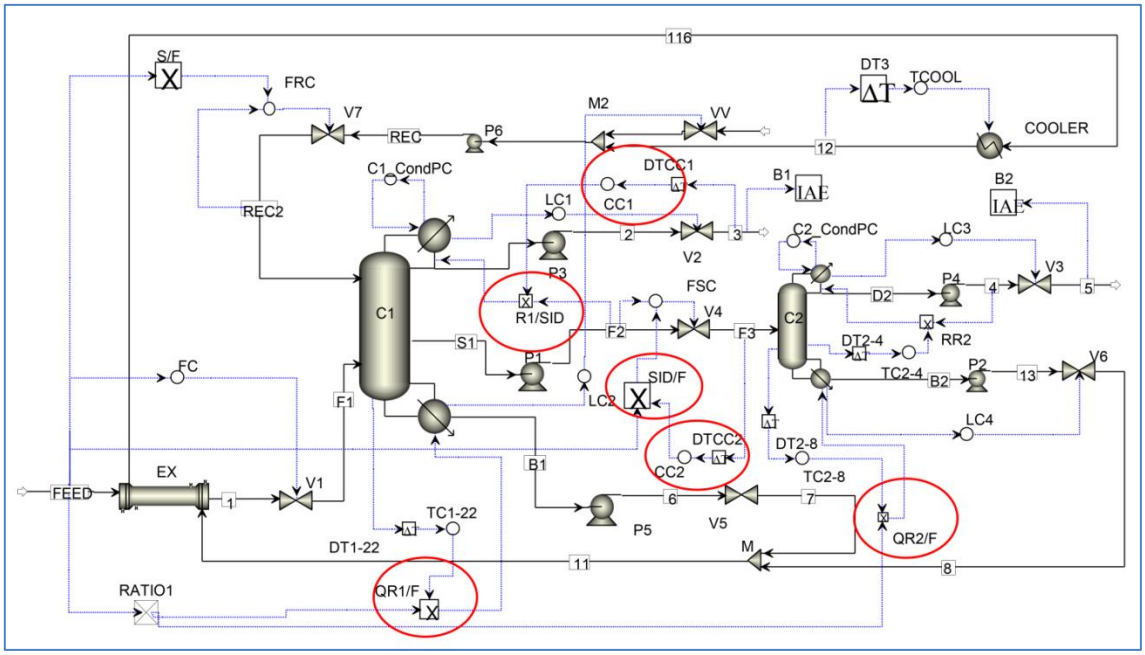

Fig. 16 The improved double-temperature control structure of the EDSH

For the control of EDSH process in which much more variables are introduced leading to converge difficultly, it could be concluded from the previous PI structures (CS1 and CS2) that there is no possibility to obtain well-handled control responses without more accurate cascade control structures. To achieve the better controllability of the SEDC, simultaneous manipulation of the flowrate of the side stream and reflux stream is the key factor. Considering the inferior performances under the condition of decreased EtAC feed composition (**Fig. 13** and **Fig. 15**), the concentration of EtAC should be applied to manipulate the ratio of reflux flowrate to side stream. Moreover, the composition controller with direct action is introduced to adjust the ratio of side stream to feed flowrate. The detailed improved CS3 is illustrated in **Fig. 16**. The "R1/SID" achieves the signal connection of reflux and side-stream flowrates. Therefore, the aim of adjusting the reflux flowrate and the side stream is simultaneously achieved and the proportion is accurately modified according to the EtAC concentration. To further enhance the dynamic performances, the "QR/F" control loops are utilized to provide the feedforward effect. The reboiler duties of the SEDC and SRC will be timely adjusted once the flowrate of the fresh feed changes. The relay-feedback tests are run again on the temperature and composition controllers and the result is summarized in **Table 9**. Of note is that the dead time for composition controllers

are 3 min while temperature controllers are 1 min.

Table 9 The tuning parameters of the temperature controllers in CS3

Controllers	**TC1-22**	**CC1**	**CC2**	**TC2-8**	**TC2-4**	**TCOOL**
Controller action	Reverse	Reverse	Direct	Reverse	Reverse	Reverse
Manipulated variable	Q_{R1}	*R1/SID*	*SID/F*	Q_{R2}	RR_2	Q_{cool}
Transmitter range	0-160.88 [a]	0-1.99	0-1.05	0-232.40 [a]	0-153.79 [a]	0-93.69 [a]
Output range	0-8.84 [b]	0-1.35	0-1.9	0-5.23 [b]	0-0.19 [b]	-3.21-0 [b]
Gain Kc	2.53	55.97	0.79	1.46	55.69	0.17
Integral time τ_I (min)	9.24	63.36	19.79	11.88	21.12	5.28

a: the units of transmitter range is "°C"

b: the units of the output range is "GJ/h"

Fig. 17 shows the dynamic responses of the improved CS3 when the feed flowrate and composition disturbances are added. All product purities are well controlled and have smaller transient deviations than CS1 and CS2. The feedforward control structure (*i.e.,* "QR/F") can dramatically improve the anti-disturbance ability for the flowrate disturbance since the transient deviation is much smaller (**Fig. 17(b)**). Most importantly, for the disturbances of decreased feed composition, the purity of EtAC is well controlled back to the setpoint in time (**Fig. 17(c)**). The purity of EtOH cannot be perfectly controlled back to the initial value under the feed composition disturbances since the purity of EtOH is controlled by the temperature rather than the composition controllers (**Fig. 17(d)**). However, the final steady-state results for the EtOH concentration are still acceptable when feed composition disturbance occurs. In summary, these results of dynamic responses indicate the CS3 can overcome the previous purity problem in EtAC after introducing the composition and "R1/SID" cascade control scheme, and as such it effectively deals with disturbances on both flowrate and composition. It is noteworthy that the proposed CS3 requires the online composition measurement for the distillated stream as well as the side stream. And there are some possible constraints of using the composition controllers such as the high cost and long measurement delay. However, with the continuous development of on-line industrial chromatography in recent years, increasing composition controllers have been applied to various processes with complexity to achieve the effective control (Qian *et al.,* 2019; Zhu *et al.,* 2019).

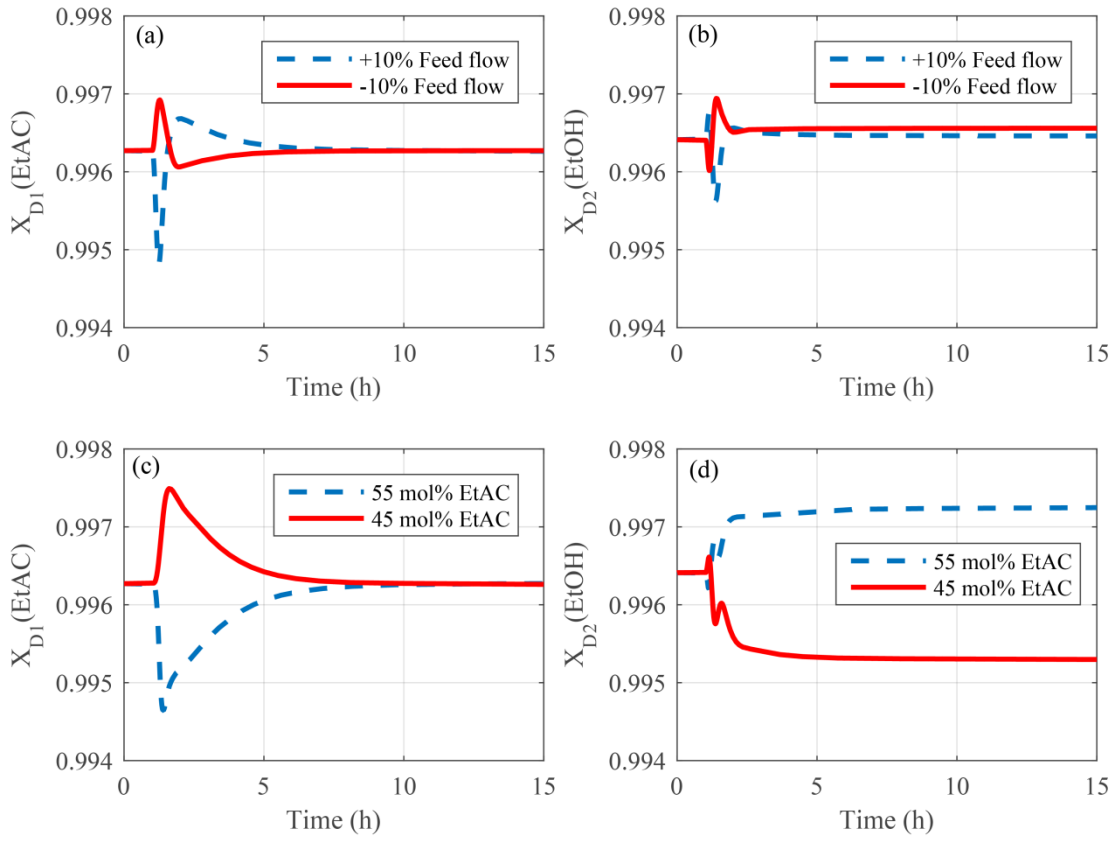

Fig. 17 The dynamic responses for the CS3 under the disturbance of ±10% feed flowrate and ±10% feed composition.

4.5 The comparison of the different control performances

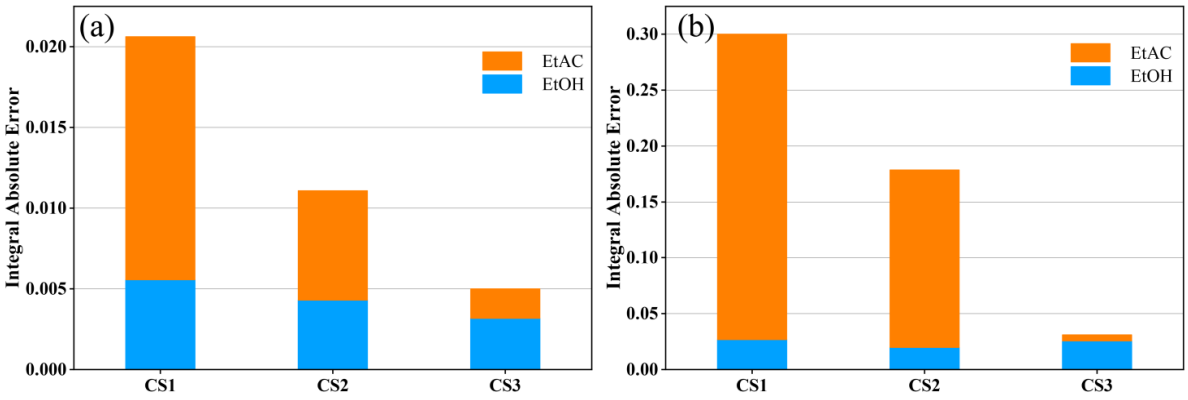

Fig. 18 The IAE comparisons of the dynamic performances of CS1, CS2 and CS3 under the disturbances of (a) ±10% feed flow rate disturbance; (b) ±10% feed composition disturbance.

To clearly compare the dynamic performances of the three control schemes, the purities of two products are employed to calculate the corresponding IAE values. And **Fig. 18** has shown the comparison of IAE for different control structures. Much lower IAE values of CS3 under the

disturbances of feed flowrate and composition indicates the best dynamic performance of CS3, which is consistent with the curves of dynamic responds shown in **Fig. 17**.

5. Conclusions

A systemic method for the energy-saving EDSH was proposed to separate minimum-boiling azeotropic mixture ethyl acetate-ethanol in this research, which involves the thermodynamic analysis based on residue curve maps, multi-objective optimization by genetic algorithm and effective side-stream control strategy for the most economic and environmental friendly process.

The application of multi-objective genetic algorithm is employed for the EDS and EDSH to obtain the optimal parameters such as the number of column stages, feed locations, side-stream location, reflux ratios and solvent flow rate. The Pareto optimal solutions of two processes provide the evidence that the EDS and the EDSH schemes can decrease the TAC by 4.54% and 7.78% respectively when compared to the conventional ED scheme. Moreover, both of the proposed EDS and EDSH can reduce the CO_2 emission by 2.74% and 9.28%, respectively. Overall, the proposed heat-integrated process exhibits its economic and environmental superiority in separating the minimum boiling azeotropic mixture EtAC/EtOH. Indeed, due to the prominent advantage of the EDSH, the dynamic controllability of EDSH is further explored. Through the comparison of the IAE of three control structures, an improved control structure for the EDSH scheme is proved to effectively deal with the feed flowrate and composition disturbances.

Of note is that the proposed design procedure can provide a general framework for other energy-saving processes for the separation of azeotropic mixtures. An attractive optimization method, genetic algorithm, could be performed to achieve the multi-objective optimization in complex chemical processes. Meanwhile, several factors such as the total energy cost, total capital cost, effects to the environment and safety evaluation can be considered simultaneously once offering more advanced optimization of genetic algorithm. The improved control structure presented in this research can provide a reference for the side-stream ED process in the industry.

Author Information

Corresponding Author

E-mail: shenweifeng@cqu.edu.cn

Notes

The authors declare no competing financial interest.

Acknowledgments

We acknowledge the financial support provided by the National Natural Science Foundation of China (Nos. 21606026, 21878028); the Fundamental Research Funds for the Central Universities (No. 2019CDQYHG021, 2019CDXYHG0013).

Appendix A

The Appendix A is available free of charge *via* the Internet.

Nomenclature

EtAC	ethyl acetate
EtOH	ethanol
EDS	side-stream extractive distillation
EDSH	side-stream extractive distillation with heat integration
TAC	total annualized cost
GA	genetic algorithm
IAE	integral absolute error
ED	extractive distillation
EDWC	extractive dividing wall column
RCMs	residue curve maps
DMSO	dimethyl sulfoxide
EDC	extractive distillation column
SEDC	side-stream distillation column
SRC	solvent recovery column
MNG	maximum number of generations
CAP	the total capital cost
ENR	the annual energy cost

References

Alcocer-García, H., Segovia-Hernández, J.G., Prado-Rubio, O.A., Sánchez-Ramírez, E., Quiroz-Ramírez, J.J., 2019. Multi-objective optimization of intensified processes for the purification of levulinic acid involving economic and environmental objectives. *Chem. Eng. Process. Proc. Intensification.* 136, 123-137.

An, Y., Li, W., Li, Y., Huang, S., Ma, J., Shen, C., Xu, C., 2015. Design/optimization of energy-saving extractive distillation process by combining preconcentration column and extractive distillation column. *Chem. Eng. Sci.* 135, 166-178.

Bortz, M., Burger, J., Asprion, N., Blagov, S., Böttcher, R., Nowak, U., Scheithauer, A., Welke, R., Küfer, K.H., Hasse, H., 2014. Multi-criteria optimization in chemical process design and decision support by navigation on Pareto sets. *Comput. Chem. Eng.* 60, 354-363.

Bravo-Bravo, C., Segovia-Hernández, J.G., Gutiérrez-Antonio, C., Durán, A.L., Bonilla-Petriciolet, A., Briones-Ramírez, A., 2010. Extractive dividing wall column: design and optimization. *Ind. Eng. Chem. Res.* 49(8), 3672-3688.

Chien, I., Kailuen Zeng, A., Chao, H.Y., 2004. Design and Control of a Complete Heterogeneous Azeotropic Distillation Column System. *Ind. Eng. Chem. Res.* 43(9), 760–765.

Chua, W.J., Rangaiah, G.P., Hidajat, K., 2017. Design and optimization of isopropanol process based on two alternatives for reactive distillation. *Chem. Eng. Process. Proc. Intensification.* 118, 108-116.

Contreras-Zarazúa, G., Sánchez-Ramírez, E., Vázquez-Castillo, J.A., Ponce-Ortega, J.M., Errico, M., Kiss, A.A., Segovia-Hernández, J.G., 2018. Inherently Safer Design and Optimization of Intensified Separation Processes for Furfural Production. *Ind. Eng. Chem. Res.* 58(15), 6105-6120.

Cui, C., Zhang, X., Sun, J., 2019. Design and optimization of energy-efficient liquid-only side-stream distillation configurations using a stochastic algorithm. *Chem. Eng. Res. Des.* 145, 48-52.

Dai, Y., Zheng, F., Xia, B., Cui, P., Wang, Y., Gao, J., 2019. Application of Mixed Solvent To Achieve an Energy-Saving Hybrid Process Including Liquid–Liquid Extraction and Heterogeneous Azeotropic Distillation. *Ind. Eng. Chem. Res.* 58(6), 2379-2388.

Douglas, J.M., 1988. Conceptual design of chemical processes. *McGraw-Hill.*

Gadalla, M.A., Olujic, Z., Jansens, P.J., Jobson, M., Smith, R., 2005. Reducing CO2 emissions and energy consumption of heat-integrated distillation systems. *Environ. Sci. Technol.* 39(17), 6860-6870.

Gerbaud, V., Rodriguez-Donis, I., Hegely, L., Lang, P., Denes, F., You, X., 2019. Review of extractive distillation. Process design, operation, optimization and control. *Chem. Eng. Res. Des.* 141, 229-271.

Ghuge, P.D., Mali, N.A., Joshi, S.S., 2017. Comparative analysis of extractive and pressure swing distillation for separation of THF-water separation. *Comput. Chem. Eng.* 103, 188-200.

Gomez, A., Pibouleau, L., Azzaro-Pantel, C., Domenech, S., Latgé, C., Haubensack, D., 2010. Multiobjective genetic algorithm strategies for electricity production from generation IV nuclear technology. *Energy Convers. Manage.* 51(4), 859-871.

Gu, J., You, X., Tao, C., Li, J., Shen, W., Li, J., 2018. Improved design and optimization for separating tetrahydrofuran–water azeotrope through extractive distillation with and without heat integration by varying pressure. *Chem. Eng. Res. Des.* 133, 303-313.

Gutiérrez-Antonio, C., Briones-Ramírez, A., 2009. Pareto front of ideal Petlyuk sequences using a multiobjective genetic algorithm with constraints. *Comput. Chem. Eng.* 33(2), 454-464.

Han, Z., Ren, Y., Li, H., Li, X., Gao, X., 2019. Simultaneous Extractive and Azeotropic Distillation Separation Process for Production of PODEn from Formaldehyde and Methylal. *Ind. Eng. Chem. Res.* 58(13), 5252-5260.

Hegely, L., Lang, P., 2018. Influence of entrainer recycle for batch heteroazeotropic distillation. *Front. Chem. Sci. Eng.* 12(4), 643-659.

Hu, Y., Su, Y., Jin, S., Chien, I.L., Shen, W., 2019. Systematic approach for screening organic and ionic liquid solvents in homogeneous extractive distillation exemplified by the tert-butanol dehydration. *Sep. Purif. Technol.* 211, 723-737.

Kiva, V.N., Hilmen, E.K., Skogestad, S., 2003. Azeotropic phase equilibrium diagrams: a survey. *Chem. Eng. Sci.* 58(10), 1903-1953.

Lai, I.K., Hung, S.B., Hung, W.J., Yu, C.C., Lee, M.J., Huang, H.P., 2007. Design and control of reactive distillation for ethyl and isopropyl acetates production with azeotropic feeds. *Chem.*

Eng. Sci. 62(3), 878-898.

Lang, Y., Biegler, L.T., 1987. A unified algorithm for flowsheet optimization. *Comput. Chem. Eng.* 11(2), 143-158.

Liang, S., Cao, Y., Liu, X., Li, X., Zhao, Y., Wang, Y., Wang, Y., 2017. Insight into pressure-swing distillation from azeotropic phenomenon to dynamic control. *Chem. Eng. Res. Des.* 117, 318-335.

Luo, H., Bildea, C.S., Kiss, A.A., 2015. Novel Heat-Pump-Assisted Extractive Distillation for Bioethanol Purification. *Ind. Eng. Chem. Res.* 54(7), 2208-2213.

Luyben, W.L., 2006. Evaluation of criteria for selecting temperature control trays in distillation columns. *J. Process Control.* 16(2), 115-134.

Luyben, W.L., 2008. Comparison of Extractive Distillation and Pressure-Swing Distillation for Acetone−Methanol Separation. *Ind. Eng. Chem. Res.* 47(8), 2696-2707.

Luyben, W.L., 2013a. Comparison of extractive distillation and pressure-swing distillation for acetone/chloroform separation. *Comput. Chem. Eng.* 50, 1-7.

Luyben, W.L., 2013b. Distillation Design and Control Using Aspen™ Simulation. *John Wiley & Sons.*

Luyben, W.L., 2017. Control of a triple-column pressure-swing distillation process. *Sep. Purif. Technol.* 174, 232-244.

Ma, K., Yu, M., Dai, Y., Ma, Y., Gao, J., Cui, P., Wang, Y., 2019. Control of an energy-saving side-stream extractive distillation process with different disturbance conditions. *Sep. Purif. Technol.* 210, 195-208.

Ma, S., Shang, X., Zhu, M., Li, J., Sun, L., 2019. Design, optimization and control of extractive distillation for the separation of isopropanol-water using ionic liquids. *Sep. Purif. Technol.* 209, 833-850.

Mitra, K., Gopinath, R., 2004. Multiobjective optimization of an industrial grinding operation using elitist nondominated sorting genetic algorithm. *Chem. Eng. Sci.* 59(2), 385-396.

Olujić, Ž., Sun, L., de Rijke, A., Jansens, P.J., 2006. Conceptual design of an internally heat integrated propylene-propane splitter. *Energy.* 31(15), 3083-3096.

Pan, H., Wu, X., Qiu, J., He, G., Ling, H., 2019. Pressure compensated temperature control of

Kaibel divided-Wall column. *Chem. Eng. Sci.* 203, 321-332.

Qian, X., Huang, K., Jia, S., Chen, H., Yuan, Y., Zhang, L., Wang, S., 2019. Composition–Temperature Cascade Control of Dividing-Wall Distillation Columns by Combining Model Predictive and Proportional–Integral Controllers. *Ind. Eng. Chem. Res.* 58(11), 4546-4559.

Rezende, M.C.A.F., Costa, C.B.B., Costa, A.C., Maciel, M.R.W., Filho, R.M., 2008. Optimization of a large scale industrial reactor by genetic algorithms. *Chem. Eng. Sci.* 63(2), 330-341.

Shen, W., Benyounes, H., Gerbaud, V., 2013. Extension of thermodynamic insights on batch extractive distillation to continuous operation. 1. Azeotropic mixtures with a heavy entrainer. *Ind. Eng. Chem. Res.* 52(12), 4606-4622.

Shen, W., Dong, L., Wei, S.A., Li, J., Benyounes, H., You, X., Gerbaud, V., 2015. Systematic design of an extractive distillation for maximum-boiling azeotropes with heavy entrainers. *AIChE J.* 61(11), 3898-3910.

Shen, W., Gerbaud, V., 2013. Extension of thermodynamic insights on batch extractive distillation to continuous operation. 2. Azeotropic mixtures with a light entrainer. *Ind. Eng. Chem. Res.* 52(12), 4623-4637.

Shi, T., Yang, A., Jin, S., Shen, W., Wei, S.A., Ren, J., 2019. Comparative optimal design and control of two alternative approaches for separating heterogeneous mixtures isopropyl alcohol-isopropyl acetate-water with four azeotropes. *Sep. Purif. Technol.* 225, 1-17.

Su, Y., Jin, S., Zhang, X., Shen, W., Eden, M.R., Ren, J., 2020. Stakeholder-oriented multi-objective process optimization based on an improved genetic algorithm. *Comput. Chem. Eng.* 132, 106618.

Tututi-Avila, S., Medina-Herrera, N., Hahn, J., Jiménez-Gutiérrez, A., 2017. Design of an energy-efficient side-stream extractive distillation system. *Comput. Chem. Eng.* 102, 17-25.

Vazquez–Castillo, J.A., Venegas–Sánchez, J.A., Segovia–Hernández, J.G., Hernández-Escoto, H., Hernández, S., Gutiérrez–Antonio, C., Briones–Ramírez, A., 2009. Design and optimization, using genetic algorithms, of intensified distillation systems for a class of quaternary mixtures. *Comput. Chem. Eng.* 33(11), 1841-1850.

Wang, C., Guang, C., Cui, Y., Wang, C., Zhang, Z., 2018a. Compared novel thermally coupled

extractive distillation sequences for separating multi-azeotropic mixture of acetonitrile/benzene/methanol. *Chem. Eng. Res. Des.* 136, 513-528.

Wang, C., Wang, C., Cui, Y., Guang, C., Zhang, Z., 2018b. Economics and Controllability of Conventional and Intensified Extractive Distillation Configurations for Acetonitrile/Methanol/Benzene Mixtures. *Ind. Eng. Chem. Res.* 57(31), 10551-10563.

Wang, Z., Su, Y., Shen, W., Jin, S., Clark, J.H., Ren, J., Zhang, X., 2019. Predictive deep learning models for environmental properties: the direct calculation of octanol-water partition coefficients from molecular graphs. *Green Chem.* 21(16), 4555-4565.

Yang, A., Lv, L., Shen, W., Dong, L., Li, J., Xiao, X., 2017. Optimal Design and Effective Control of the tert-Amyl Methyl Ether Production Process Using an Integrated Reactive Dividing Wall and Pressure Swing Columns. *Ind. Eng. Chem. Res.* 56(49), 14565-14581.

Yang, A., Shen, W., Wei, S.A., Dong, L., Li, J., Gerbaud, V., 2019a. Design and control of pressure-swing distillation for separating ternary systems with three binary minimum azeotropes. *AIChE J.* 65(4), 1281-1293.

Yang, A., Shi, T., Sun, S., Wei, S.A., Shen, W., Ren, J., 2019b. Dynamic controllability investigation of an energy-saving double side-stream ternary extractive distillation process. *Sep. Purif. Technol.* 225, 41-53.

Yang, A., Sun, S., Eslamimanesh, A., Wei, S.A., Shen, W., 2019c. Energy-saving investigation for diethyl carbonate synthesis through the reactive dividing wall column combining the vapor recompression heat pump or different pressure thermally coupled technique. *Energy.* 172, 320-332.

Yang, A., Wei, R., Sun, S., Wei, S.A., Shen, W., Chien, I.L., 2018. Energy-Saving Optimal Design and Effective Control of Heat Integration-Extractive Dividing Wall Column for Separating Heterogeneous Mixture Methanol/Toluene/Water with Multiazeotropes. *Ind. Eng. Chem. Res.* 57(23), 8036-8056.

Yang, A., Zou, H., Chien, I.L., Wang, D., Wei, S.A., Ren, J., Shen, W., 2019c. Optimal Design and Effective Control of Triple-Column Extractive Distillation for Separating Ethyl Acetate/Ethanol/Water with Multiazeotrope. *Ind. Eng. Chem. Res.* 58(17), 7265-7283.

Yi, C.C., Shen, W., Chien, I.L., 2018. Design and control of an energy-efficient alternative

process for the separation of methanol/toluene/water ternary azeotropic mixture. *Sep. Purif. Technol.* 207, 489-497.

You, X., Gu, J., Gerbaud, V., Peng, C., Liu, H., 2018. Optimization of pre-concentration, entrainer recycle and pressure selection for the extractive distillation of acetonitrile-water with ethylene glycol. *Chem. Eng. Sci.* 177, 354-368.

Zhang, Q., Liu, M., Li, C., Zeng, A., 2018. Design and control of extractive distillation process for separation of the minimum-boiling azeotrope ethyl-acetate and ethanol. *Chem. Eng. Res. Des.* 136, 57-70.

Zhang, Q., Liu, M., Zeng, A., 2019. Performance enhancement of pressure-swing distillation process by the combined use of vapor recompression and thermal integration. *Comput. Chem. Eng.* 120, 30-45.

Zhao, Y., Ma, K., Bai, W., Du, D., Zhu, Z., Wang, Y., Gao, J., 2018. Energy-saving thermally coupled ternary extractive distillation process by combining with mixed entrainer for separating ternary mixture containing bioethanol. *Energy.* 148, 296-308.

Zhu, Z., Geng, X., Li, G., Yu, X., Wang, Y., Cui, P., Tang, G., Gao, J., 2019. Control comparison of extractive distillation with two different solvents for separating acetone and tetrahydrofuran. *Process Saf. Environ. Prot.* 125, 16-30.

Zhu, Z., Xu, D., Liu, X., Zhang, Z., Wang, Y., 2016. Separation of acetonitrile/methanol/benzene ternary azeotrope via triple column pressure-swing distillation. *Sep. Purif. Technol.* 169, 66-77.